Systematic Analysis of Biological Processes Reveals Gene Co-expression Modules Driving Pathway Dysregulation in Alzheimer's Disease

Temitope Adeoye[1], Syed I Shah[1], and Ghanim Ullah[1,*]

[1]Department of Physics, University of South Florida, Tampa, FL 33620.

[*]Correspondence: gullah@usf.edu

Abstract

Background

Alzheimer's disease (AD) manifests as a complex systems pathology with intricate interplay among various genes and biological processes. Traditional differential gene expression (DEG) analysis, while commonly employed to characterize AD-driven perturbations, does not sufficiently capture the full spectrum of underlying biological processes. Utilizing single-nucleus RNA-sequencing data from postmortem brain samples across key regions—middle temporal gyrus, superior frontal gyrus, and entorhinal cortex—we provide a comprehensive systematic analysis of disrupted processes in AD. We go beyond the DEG-centric analysis by integrating pathway activity analysis with weighted gene co-expression patterns to intricately map gene interconnectivity, identifying region- and cell-type-specific drivers of biological processes associated with AD. Our analysis reveals profound modular heterogeneity in neurons and glia as well as extensive AD-related functional disruptions. Co-expression networks highlighted the extended involvement of astrocytes and microglia in biological processes beyond neuroinflammation, such as calcium homeostasis, glutamate regulation, lipid metabolism, vesicle-mediated transport, and TOR signaling. We find limited representation of DEGs within dysregulated pathways across neurons and glial cells, suggesting that differential gene expression alone may not adequately represent the disease complexity. Further dissection of inferred gene modules revealed distinct dynamics of hub DEGs in neurons versus glia, suggesting that DEGs exert more impact on neurons compared to glial cells in driving modular dysregulations underlying perturbed biological processes. Interestingly, we observe overall downregulation of both astrocyte and microglia modules in AD across all brain regions, indicating a prevailing trend of functional repression in glial cells across these regions. Notable genes belonging to the CALM and HSP90 family genes emerged as hub genes across neuronal modules in all brain regions, suggesting conserved roles as drivers of synaptic dysfunction in AD. Our findings demonstrate the importance of an integrated, systems-oriented approach combining pathway and network analysis for a comprehensive understanding of the cell-type-specific roles of genes in AD-related biological processes.

Keywords

Alzheimer's disease, single-nucleus RNA-sequencing, biological processes, gene co-expression modules, pathway dysregulation, systems analysis, hub genes.

Background

Alzheimer's disease (AD) is an increasingly prevalent neurodegenerative disorder with global cases surpassing 50 million, presenting an urgent need for understanding its complex pathology (1,2). The etiology of AD is characterized by hallmark molecular and cellular alterations, most notably the accumulation of senile amyloid-beta (Aβ) plaques and the presence of hyperphosphorylated Tau neurofibrillary tangles (NFTs) (2–6). Such pathological alterations often trigger neurotoxic cascades, resulting in synaptic dysfunction, pervasive neuronal loss, and subsequent functional disruption of neuronal networks (7–11). However, AD perturbations manifest heterogeneously across brain regions and cell types, contributing to the complexity of its pathology (12,13). Indeed, several lines of evidence indicate that AD inflicts selective disruptions to biological processes among cellular subpopulations in different brain regions, revealing a region- and cell-type-dependent susceptibility (14–17). This cellular and regional diversity in affected mechanisms poses significant challenges in the discovery and screening of candidate biomarkers and potential therapeutic strategies.

Recent advancements in single-cell/single-nucleus RNA-sequencing (sc/snRNA-seq) present an opportunity to dissect the molecular basis of AD with unprecedented resolution (18,19). Leveraging these techniques, numerous studies have identified differential gene expression (DEG) patterns associated with AD, revealing insights into cellular states and their variations during disease progression (20–23). For instance, gene expression analysis of cells in the prefrontal cortex revealed that neurons primarily contain downregulated genes in AD, while glial cells, albeit to a lesser extent, exhibit opposite directionality (21). Indeed, top DEGs were cell type-specific, highlighting the distinct cell-type-specific transcriptional responses to AD-associated perturbations. Consistent with this, Grubman et al.(24) identified upregulated transcription factors in the entorhinal cortex that mediate cell-type-specific state transitions from control to AD. Similarly, comprehensive transcriptomic evaluations in human and mice models revealed a unique set of DEGs associated with a disease-associated microglia (DAM) state (22,23,25). Notably, these studies revealed that the DAM state is marked by downregulation of several homeostatic genes, recapitulating the notion that cell-type subpopulations can express distinct transcriptional alterations. Recently, Habib et al. (26) reported an AD-associated astrocyte subpopulation in the prefrontal cortex and hippocampus, characterized by elevated GFAP levels and increased expression of genes implicated in amyloid aggregation and inflammation (22,26). Despite the detailed transcriptional landscape of AD outlined by these findings, such investigations predominantly focus on isolated differential gene expressions, lacking an integrated systems-level understanding of the relationships between these genes and their functions within broader biological processes.

AD is recognized as a systems disease, where the pathology extends beyond molecular alterations to encompass complex interactions in gene networks (27,28). The pathological progression and

perturbation of biological processes in AD are not merely driven in isolation by DEGs, but rather by the complex interplay of a robust sets of genes within biological processes or signaling cascades (29). Thus, the collective molecular interactions observed across various cellular processes fundamentally shape the pathogenesis of AD (30). Gene co-expression network analyses have emerged as critical tools to capture these interactions, uncovering highly interconnected network of genes in AD and higher order network structures associated with the pathology. Notably, Morabito et al. (31) utilized this systems-level perspective to identify consensus networks of microglia genes representing classical markers of homeostatic microglia or known DAM genes, indicating that microglia assume activated states due to the functional interplay of associated genes. Likewise, Miyoshi et al. (32) demonstrated unique dysregulation patterns in functional biological units in early sporadic AD, suggesting that dynamic modular changes in gene expression may play a crucial role in AD progression. These findings collectively offer a thorough characterization of the systems-level features of the AD brain. However, since functional perturbation of biological processes arises from the underlying network architecture of the comprising gene programs, it is still unclear whether and to what extent DEGs play a central role in the perturbation of these processes or whether they are merely partakers of their associated biological units (33,34).

In this study, we leverage snRNA-seq data from key regions of postmortem AD brains to conduct a systems-level analysis of pathway perturbations. Our approach integrates pathway activity analysis with weighted gene co-expression patterns, providing insights into functional coherence and interplay among genes involved in perturbed biological processes in AD. To identify the complex systems-level changes in both neuronal and glial cell populations, we first comprehensively characterize region- and cell-type-specific pathway dysregulation patterns associated with AD. This nuanced approach reveals an expanded role for astrocytes and microglia in a variety of biological processes than previously appreciated in neuron-centric models of AD. We also highlight the dysregulation of calcium (Ca^{2+}) signaling across different cell types and regions, representing an axis of disruption that has been consistently implicated in AD pathology. Next, we qualitatively demonstrate that DEGs are not robustly distributed in the curated set of genes comprising the biological processes (gene programs) implicated in AD. Finally, we employ a weighted gene co-expression strategy to uncover gene modules and highly connected hub genes underlying the perturbed gene programs. This approach revealed distinct dynamics of hub DEGs (hub-DEGs) in neuronal versus glial modules, which suggests that DEGs exert a more pronounced influence on neurons than on glial cells in driving pathway perturbations in AD. By offering a comprehensive, systems-driven perspective of AD pathology, our findings refine the current understanding of the disease and opens new avenues for targeted therapeutic and diagnostic strategies.

Methods

Study Design and Data Acquisition

Here, we leveraged pre-processed snRNA-seq data obtained from two independent studies (20,35) comprising three different brain regions: Middle Temporal Gyrus (MTG), Superior Frontal Gyrus (SFG), and Entorhinal Cortex (ETC) (*Fig. 1*). We reasoned that using samples matched for pathological status would minimize the technical variation due to data composition and allow for meaningful comparison across the brain regions. To accomplish this, we selected a cohort of 10 male individuals form the Gabitto et al. (MTG) (35) study based on their level of AD neuropathologic change (ADNC). Donors from the Gabitto et al. study (35) were specifically chosen to align with corresponding cases from the Leng et al. (SFG & ETC) study (20). ADNC stage is evaluated using the robust "ABC" scoring system, considering the Thal phases (A) to gauge the overall Aβ burden; Braak stage (B) for neurofibrillary tangles (NFT) load, and neuritic plaque score (C) (36). The combination of A, B, and C scores are used to categorize individuals into distinct pathological stages, denoted as "Not AD", "Low", "Intermediate" and "High" ADNC stages. It is worth mentioning that accumulation of Aβ plaques and extent of NFT inclusions have consistently proven to be the most reliable correlates of neuropathological staging and AD diagnosis (37–39). Consequently, "Intermediate" or "High" AD neuropathologic stages are typically associated with dementia. To ensure a balanced representation across ADNC stages, each study cohort comprised four individuals with a "Not AD" descriptor, representing cognitively healthy controls, while the remaining six were equally distributed among Low/Intermediate and High ADNC stages, allowing us to capture the cortical-free, early, and late stages of AD pathology in our analysis (*Fig. 1*). The pre-processed data (obtained after quality-control filtering) from (35) contained 154,368 snRNA-seq profiles from the MTG, while a total of 106,136 nuclei (SFG = 63,608 & ETC = 42,528) were obtained from (20) (*Fig. 1*). Predefined cell-type annotations were used to restrict analysis to six different cell types: excitatory neurons, inhibitory neurons, astrocytes, microglia, oligodendrocytes, and oligodendrocyte precursor cells (OPCs).

The overall cohort of 20 male individuals were originally enrolled in the Adult Changes in Thought (ACT) Study, the University of Washington Alzheimer's Disease Research Center (ADRC) (35), the Neurodegenerative Disease Brain Bank (NDBB) at UCSF, or the BBAS from the University of Sao Paulo (20,40). These individuals were part of a larger cohort previously reported in (20,35). Notably, brain specimens from the Leng et al. study (20) were obtained from NDBB and BBAS, representing 10 of the male participants from the postmortem cohort used in this study. Brain slices were obtained from ETC and SFG (Brodmann area 8). All individuals underwent rigorous neuropathological assessments following established protocols, ensuring that selected brain samples exhibited pronounced AD-type pathology while excluding non-AD pathologies, such as Lewy body disease, TDP-43 proteinopathies, primary tauopathies, and cerebrovascular changes.

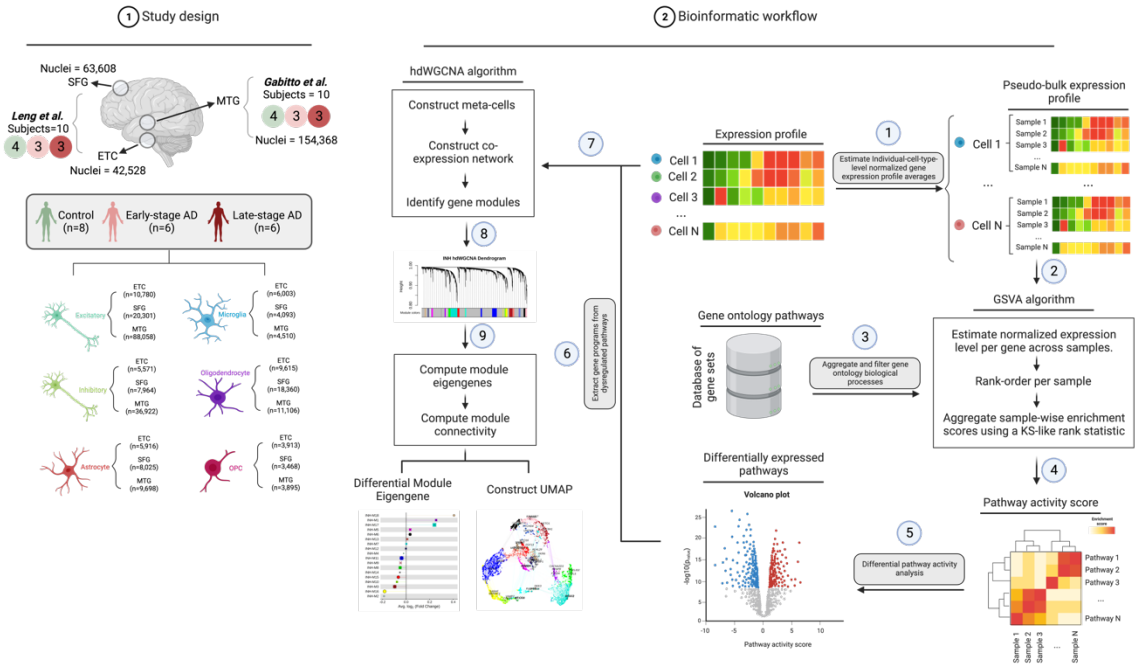

Fig. 1. Schematic overview of study workflow and analytical methods. *Sample and nuclei distribution across pathological and study groups are shown in the left panel, while the right panel illustrates the bioinformatics pipeline employed for the identification of perturbed gene ontology (GO) biological processes and their associated gene co-expression networks (**Methods**), created using BioRender.com. The workflow begins with computing pseudo-bulked averages of normalized gene expression profiles for single-cell expression profiles of each cell type (Steps 1 & 2). Subsequently, pathway activity scores were calculated (Steps 3 & 4), using gene set variation analysis (GSVA) as previously described (41). Differential pathway activity was then estimated for each pathway-cell type combination, employing a multivariate linear model (Step 5). Construction of co-expression networks, performed with hdWGCNA (31) was specifically limited to gene programs comprising perturbed pathways (Steps 6—8).*

The study cohort comprised 10 male participants subjected to snRNA-seq, presenting a diverse spectrum of Braak stages (ranging from 0 to 6), ADNC categories (comprising Not AD [n=4], Low [n=3], and High [n=3]), and consistently harboring APOE ε3/ε3 genotypes. The isolation of nuclei was extensively documented in (20). Briefly, postmortem frozen brain tissue was dounce-homogenized with the addition of IGEPAL-630, followed by gradient centrifugation for nuclei filtration and purification. Subsequently, sequencing libraries were constructed utilizing droplet-based snRNA-seq with 10X Genomics' Chromium Single Cell 3' Reagent Kits v2, targeting a total of 10,000 nuclei per sample. The resulting sequencing data underwent demultiplexing through Cell Ranger, utilizing a customized pre-

mRNA GRCh38 reference genome designed to accommodate introns. Alignment and gene expression quantification were performed using cellranger count under default settings.

Brain specimens from the study by Gabitto et al. (35) were obtained from the ACT Study and the UW ADRC. The study cohort was carefully selected, encompassing a wide spectrum of AD severity while excluding individuals diagnosed with Frontotemporal Dementia, Frontotemporal Lobar Degeneration, Down Syndrome, Amyotrophic Lateral Sclerosis, or other degenerative disorders (except Lewy Body Disease). The cohort consisted of 84 participants aged 65 and above, representing various stages of Alzheimer's disease severity. Rapid autopsies were conducted to ensure a postmortem interval of less than 12 hours. Tissue processing involved uniform coronal slicing of one hemisphere, fixed or frozen slabs, and subsequent processing of Superior and Middle Temporal Gyrus tissue samples. As in (20), the study rigorously adhered to neuropathological assessments, tissue processing, and immunohistochemical analyses, providing clinical, cognitive, and demographic data. Specifically, the study comprised a cohort of 84 ACT/ADRC donors spanning a broad range of ADNC levels and comorbid pathologies, including Lewy Body Disease, vascular brain injury, and hippocampal sclerosis. Notably, the cohort tended to skew towards more advanced stages of the disease, with 58% of participants exhibiting a Braak stage of 5 or higher (Braak Stage: 0 [n=2], 2 [n=4], 3 [n=6], 4 [n=23], 5 [n=34], 6 [n=15]) and 61% having a Thal Phase of 4 or higher (Thal Phase: 0 [n=9], 1 [n=5], 2 [n=7], 3 [n=12], 4 [n=30], 5 [n=21]). Demographically, the cohort displayed a slight female bias (51 females and 33 males), particularly among donors with high ADNC (Not AD [N=9], Low [n=12], Intermediate [n=21], High [n=42]). Furthermore, the cohort was characterized by advanced age, with an average age at death of 88 years, and half of the donors received a clinical diagnosis of dementia. Genetic analysis revealed the presence of the APOE ε4 genotype, a primary risk factor for AD, in 23 donors, while the remaining donors possessed ε3 and ε2 alleles in various combinations. Sequencing libraries were constructed following standard guidelines for 10x Genomics kits. RNA isolation from nuclei was performed with subsequent evaluation of RNA integrity. The isolated nuclei and high-quality RNA samples were then employed for snRNA-seq, snATAC-seq, and MERFISH. The selection of individuals from this study for our work was based on their alignment with corresponding cases from the participants in (20), considering their level of ADNC. For the present analysis, participants were stratified based on the ADNC spectrum, encompassing individuals from "Not AD" to various stages of AD pathology as outlined above.

Data Processing

The processed droplet-based snRNA-seq profiles, amounting to a total of 260,504 profiles, were obtained from (42,43). Quality control and filtering steps were previously detailed in each study. In Leng et al. (20), raw gene-barcode matrices were converted into SingleCellExperiment (SCE) objects in R using DropletUtils. Nuclei from empty droplets or with fewer than 200 UMIs were discarded,

203 followed by data merging and normalization based on the strategy in (44). High-variance genes were
204 identified for dimensionality reduction using the Seurat package, but as individual origin influenced
205 results, the scAlign tool was adopted for cross-sample alignment, prioritizing biological over technical
206 factors. Clusters were mapped to major brain cell types using specific marker genes, with ambiguous
207 clusters removed, and fine-grained subclustering performed by isolating cells from primary cell types.
208 In the study Gabitto et al. (35), nuclei gene expression data were mapped to a reference transcriptome
209 using gene expression and chromatin accessibility profiles, discarding nuclei with fewer than 500
210 detected genes from upstream of cell type mapping. The filtered nuclei were then classified into classes,
211 subclasses, and supertypes using scANVI, with predictions evaluated against known marker gene
212 expressions. Regions with variable expression were examined for potential contamination, and data
213 were further refined using high-resolution Leiden clustering. Clusters with undesirable metrics were
214 subsequently flagged and removed to further improve quality.

215 The samples from the ETC and SFG of autopsied brains generated by Leng et al. (20) is accessible for
216 download from Synapse.org (42) under the Synapse ID syn21788402. Gabitto et al. (35) data, generated
217 from the MTG, was obtained from the Seattle Alzheimer's Disease (SEA-AD) Brain Cell portal (43,45).
218 We categorized participants into three distinct groups: 8 individuals with "Not AD" designation served
219 as cognitively healthy controls, while 12 individuals manifested mild to severe AD-pathology. Out of
220 these 12 AD-pathology group, 6 participants with "Low" or "Intermediate" ADNC scores are designated
221 as 'early-pathology' group, whereas the remaining 6 with a "High" ADNC scores are designated as 'late-
222 pathology' group. As reported in the source studies, informed consent was obtained for all participants,
223 and ethical approvals for the use of human tissues were obtained from the respective institutional review
224 boards. All post-mortem neuropathological assessments, clinical evaluations, and pathological
225 grouping are detailed in Supplementary Table 1.

226 ***Differential gene expression***

227 Cell type-specific differential gene expression analysis was evaluated using a customized version of the
228 Libra R package (46) accessible via GitHub. The source package implements 22 unique differential
229 expression methods that can all be accessed from a singular function call. Given the susceptibility of
230 cell-based differential expression methods to the drop-out events and overdispersion intrinsic to single-
231 cell data, we mitigated against these limitations by using a method designed specifically for bulk
232 sequencing data. Specifically, we adopted the DESeq2 (47) routine with the Wald test for differential
233 expression analysis between the control group and the AD group. To ensure that the analysis accounted
234 for true biological replication—that is variability at the level of individual objects—unique molecular
235 identifier (UMI) counts from cells belonging to the same individual and specific cell type were
236 aggregated to create 'pseudo-bulk' samples. Genes with negligible expression in a given cell type,
237 indicated by a nonzero detection rate below 10% in the aggregated pseudo-bulk, were precluded from

further analyses to mitigate false-positive discoveries. Preliminary assessment of the principal components of these individual-level aggregated gene expression profiles corroborated the decision to exclude additional covariates, such as age at death and post-mortem interval. Therefore, the pathological status served as the sole covariate in our differential expression model. Genes were identified as significantly differentially expressed if they exhibited an absolute log fold change exceeding 0.25 and a false discovery rate (FDR) below 0.01. The table of p-values and log fold changes for all genes across all brain regions and cell types is provided in Supplementary Tables 2—4.

Pathway analyses

The compendium of Gene Ontology biological processes (2018 edition) was retrieved from the Mayaan laboratory repository (48). Certain pathways were renamed to optimize clarity and standard nomenclature, with specific modifications enumerated in Supplementary Table 5.

Pathway activity scores were computed in accordance with protocols outlined in (49). This method effectively retrieved cell type-specific signatures, not accounted for by randomly sampled gene set enrichment analysis (50). In brief, we first computed cell-type-level normalized gene expression profiles for each individual using the ACTIONet normalization procedure (51). Subsequently, pathway activity scores were computed as previously implemented in the R package GSVA (version 1.46.0) (41). GSVA executed with the following parameters: mx.diff=TRUE, kcdf=c("Gaussian"), min.sz=5, max.sz=500. To minimize the discovery of false positive, gene sets were filtered to exclude genes with insufficient expression in the designated cell type, defined by a nonzero detection rate less than 10%. For each pathway and cell type, activity scores were modeled using a multivariate linear regression, taking the form: activity score $\sim\beta_0 \times$ *pathology.group*. No additional covariates were incorporated, as PCA revealed no significant association with pathological status, thus not accounting for observed variances in overall gene profiles. The "pathology.group" variable stratifies samples into 'no-pathology,' 'early-pathology,' or 'late-pathology' categories. Linear models were fitted using the lmfit() function, and corresponding t-statistics were generated through the eBayes() function, both from the Limma R package (version 3.50.3). Differential expression between the 'no-pathology' and 'AD-pathology' groups was estimated by setting the contrast argument as *makeContrast = (early + late)/2 – no*. Pathways were identified as significantly differentially expressed based on a nominal p-value cut-off of 0.05 (as depicted in Figure 1). The procedure resulted in the identification of prioritized candidate pathways across major cell types. Estimates of β_0 coefficients, along with additional statistics as outlined in Figure 1, are comprehensively documented in Supplementary Tables 6—8, including both nominal p-values and FDR-corrected p-values.

Gene Co-expression Network Analysis

Network construction and module identification

To generate robust gene-gene correlations, we employed hdWGCNA (version 0.2.18) (31), specifically tailored for single-cell and scRNA-seq data. We first generated a Seurat object (version 4.3.0.1) (52) using the `SetupForWGCNA` function, setting the "gene_select" parameter to custom. We confined our analysis to functionally relevant gene programs, extracted from the gene sets comprising the pathways that were dysregulated (with nominal p-values less than 0.05) in each cell type. Metacells, which are essentially aggregates of transcriptionally similar cells originating from the same biological replicate, were constructed using the k-Nearest Neighbors (KNN) algorithm, with default parameters (k=25, max_shared=10). This step mitigated data sparsity inherent to scRNA-seq data and generated a metacell gene expression matrix conducive for robust network construction. Subsequently, the optimal soft power threshold was determined using TestSoftPowers function in a 'signed' network, conducting a parameter sweep over a range of 1 to 30. This specifies the degree to which gene-gene correlations are scaled in order to reduce the amount of noise present in the correlation matrix and prioritize strong correlations. The selected soft power thresholds, demonstrating a fit to the scale-free topology model, are reported in Supplementary Figures 3—5. Network construction and module detection were performed using the ConstructNetwork function, which employs the scaled correlations to compute a topological overlap matrix (TOM), reflecting the network of shared neighbors between genes. Module dendrograms were visualized using the PlotDendrogram function (Supplementary Figures 6—8).

Module signatures and hub gene identification

To summarize the gene signatures within each module, module eigengenes (ME) were calculated using the ModuleEigengenes function with default settings. This effectively represents the first principal components of the subset of the gene expression matrix comprising each module, allowing us to obtain the module feature genes. The intra-modular connectivity (kME), a metric representing the correlation of each gene with its ME, was determined using the SignedKME algorithm, essentially determining the highly connected genes in each module.

Network visualization

For a comprehensive low-dimensional visualization, we applied the RunModuleUMAP function on the TOM, confining it to the top 5 hub genes per module based on kME values. This resulted in a UMAP representation where the organization was primarily determined by the hub genes, and only the top 10 hub genes in each module were annotated in the UMAP space.

304 ***Differential module analysis and functional enrichment***

305 To discern modular differences between control and diseased group in each cell type, a differential
306 module eigengene analysis was performed using the FindAllMarkers function in Seurat, applying the
307 Wilcoxon test. Results are depicted in lollipop diagrams, with non-significant modules marked "X"
308 (nominal $P > 0.05$). Supplementary Tables 9—11 contains additional statistics for each cell type across
309 tested brain regions. Furthermore, the overlap of co-expression modules with DEGs or AD-associated
310 genes from the Open Targets Platform (53), KEGG Alzheimer's disease pathways (54), and
311 Harmonizome (55) was calculated using the R package GeneOverlap (version 1.34.0) via Fisher's exact
312 test. Finally, functional enrichment analysis was conducted on hdWGCNA modules using the R
313 package enrichR, focusing on Gene Ontology processes exhibiting differential expression in specific
314 cell types.

315

316

317

318

319

320

321

322

323

324

325

326

327

Results

Cell-type- and region-specific perturbations in molecular processes define the heterogeneous responses to AD

To comprehensively characterize perturbed molecular processes in AD, we performed differential pathway activity analysis, leveraging Gene Ontology biological processes (*Fig. 1*, **Methods**). To enhance the sensitivity in detecting subtle changes in pathway activity, we first aggregated gene expression values into pathway activity scores (*Fig. 1*, **Methods**) (49). These scores effectively summarize the collective gene expression levels within each pathway and improved statistical power for subsequent analyses. We then examine whether there are qualitative changes in the aggregated scores due to AD using a multivariate linear model with pathological status as the only covariate. Preliminary analysis of the principal components of the aggregated expression data revealed that other covariates, such as age at death and post-mortem interval, are not correlated with biological or technical variation (*Supplementary Fig. 1*), and as a result were excluded from the design matrix, ensuring that the data modeling focused solely on the biologically relevant factors (56). Pathology groups were defined based on the ADNC levels (Supplementary Table 1, **Methods**), with individuals categorized as early-pathology (low or intermediate ADNC) or late-pathology (high ADNC). These two groups correspond to the pathological progression of AD. early-pathology individuals have discernible amyloid load coupled with mild neurofibrillary tangles and cognitive deficit. Conversely, the late-pathology individuals show higher amyloid burden, elevated NFT deposits, pervasive pathology, and pronounced cognitive impairment (37–39). Both pathology groups were combined in the contrast analysis to assess differential expression between AD-pathology and control groups (**Methods**).

Our analysis revealed that AD inflicts a wide range of perturbations in molecular process ($P < 0.05$) across the three brain regions (*Fig. 2—4*), ranging from cell-type-specific alterations, exclusive to a single cell type (*Fig. 2*), to broadly dysregulated pathways affecting at least two cell types (*Fig 3*). Remarkably, the affected pathways displayed substantial similarity across brain regions, with some showing consistent directional changes across cell types, while others exhibited complex patterns of distinct alterations in each cell type (*Supplementary Fig. 2; see Supplementary Table 12 for full list of overlapping pathways*).

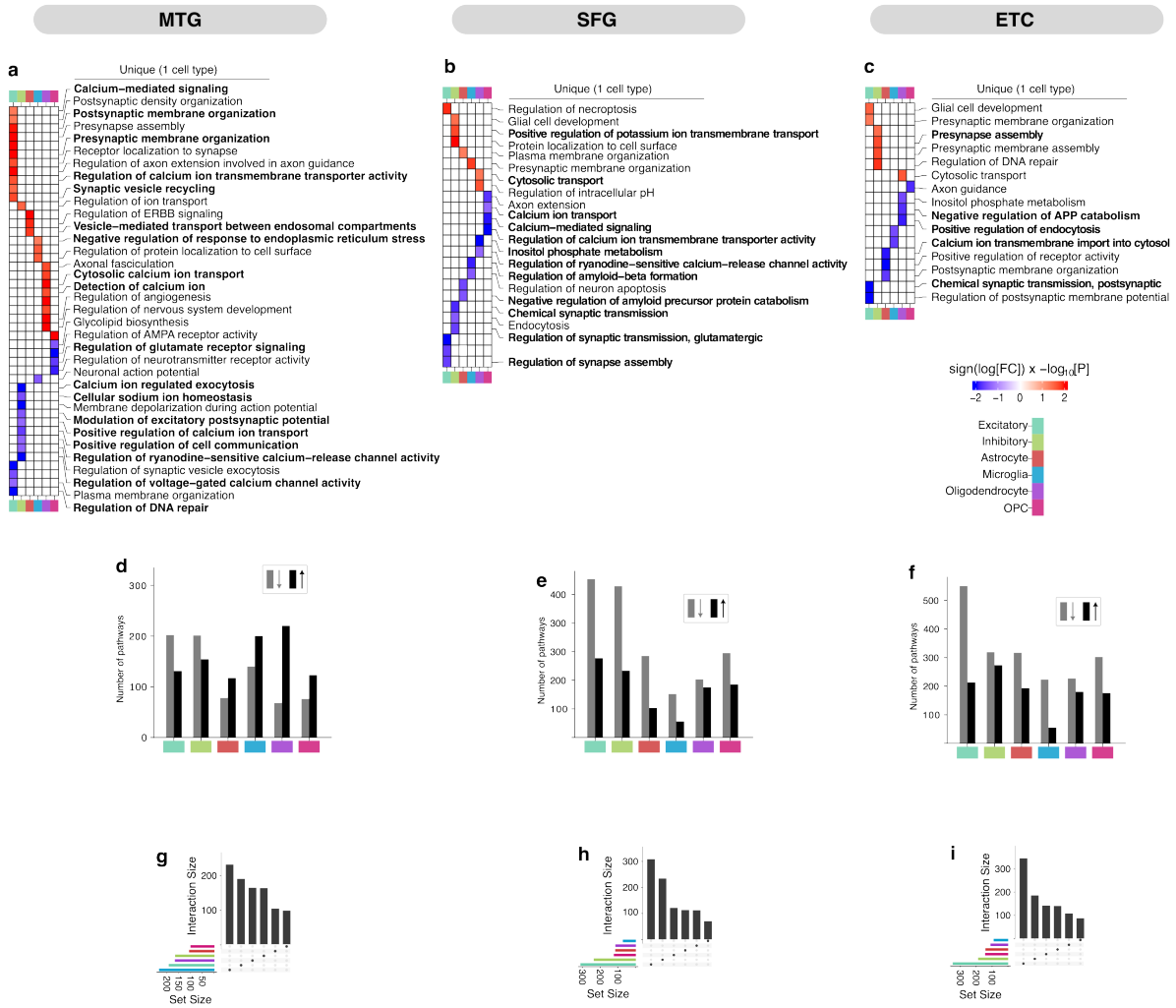

***Figure 2. Cell-type-specific pathway perturbations in AD**. (**a—c**). Heatmaps representing select Gene Ontology biological processes dysregulated in individual cell types (nominal P < 0.05). Each column represents data for a particular brain region. Unique alterations denote evidence of pathway alteration in a single cell type, with red indicating upregulation and blue signifying downregulation. Pathways discussed in the Article are highlighted in bold text. (**d—f**), Distribution of up- and down-regulated pathways across each cell type. Black indicates upregulation and grey indicates downregulation. (**g—i**), Upset plots displaying the distribution of uniquely perturbed pathways.*

Specifically, in the MTG, cell-type-specific perturbations were particularly evident in excitatory neurons, manifesting predominantly in dysregulation of synaptic-related processes, including upregulation of pre- and post-synaptic membrane organization, synaptic vesicle recycling, and Ca^{2+} -mediated synaptic signaling (*Fig. 2a*). Conversely, inhibitory neurons in the MTG showed a distinct pattern of downregulation in processes like excitatory postsynaptic potential, Ca^{2+} ion transport, and

371 cell communication. Additionally, we observed cell-type-specific dysregulations in astrocytes (vesicle-
372 mediated transport, *P=0.0149*), microglia (inflammatory response, *P=0.0003*), oligodendrocytes
373 (nervous system development, *P=0.0049*), and OPCs (TORC1 signaling, *P=0.0001*), each
374 demonstrating unique pathway alterations pertaining to their cellular functions. For instance, astrocytes
375 exhibited upregulation of endosomal-related vesicle transport, while microglia showed alterations in
376 protein localization and endoplasmic reticulum stress response (*Fig. 2a*). Oligodendrocytes were
377 affected in nervous system development, and OPCs displayed perturbed glycolipid synthesis (*Fig. 2a*).
378 However, a considerable number of processes were uniquely altered in specific cell types, highlighting
379 the highly cell type-specific nature of pathway perturbations in the MTG (*Fig. 2g*).

380 Surprisingly, synaptic-related alterations were not exclusive to neurons; Ca^{2+} ion-dependent exocytosis
381 was consistently downregulated across neuronal cells, while dysregulated neurotransmitter receptor
382 transport and internalization were observed in OPCs and inhibitory neurons, among other broadly
383 dysregulated processes (*Fig. 3a*). In addition, processes involved in the regulation of Ca^{2+} ions, voltage-
384 gated Ca^{2+} channel activity and signaling, as well as myelination, exhibited distinct patterns of
385 perturbation in excitatory, inhibitory, oligodendrocytes, and OPCs (Fig. *3g*). Notably, 60% (n=333,
386 P<0.05) and 57% of pathways are downregulated in excitatory and inhibitory neurons (n=355, P<0.05),
387 respectively. In contrast 58-76% of pathways are upregulated in astrocytes (n=195, P<0.05), microglia
388 (n=340, P<0.05), oligodendrocytes (n=287, P<0.05), and OPCs (n=199, P<0.05) (Fig. 2d). These
389 findings together highlight the highly cell type-specific nature of pathway perturbations in the MTG,
390 suggesting divergent mechanisms between neuronal and glial cells.

391 We next examined the pathway dysregulation patterns in the SFG and ETC. Similar to findings in the
392 MTG, we observed a diverse set of AD-induced pathway alterations uniquely or broadly perturbed in
393 the SFG and ETC (*Fig 2&3b,c*), further highlighting the heterogeneity of cellular responses to AD
394 pathology. These include processes like synaptic transmission and membrane organization in neurons,
395 amyloid beta formation and amyloid precursor protein (APP) catabolism in microglia, astrocytes, and
396 oligodendrocytes, and axon maintenance processes regulated by OPCs. Interestingly, all cell types in
397 both SFG and ETC exhibit a strong signature of repression, with 53-80% of pathways showing
398 downregulation. This consistent alteration pattern across all cell types suggests a more pervasive
399 disruption of molecular processes in these regions compared to the MTG. Moreover, a significant
400 proportion of processes (53% in the SFG and 55% in the ETC) were perturbed either in neurons or a
401 glial cell type, indicating a trend toward broader AD-driven disruption of molecular processes in the
402 ETC and SFG (*Fig 3d—f*). Indeed, top differentially expressed pathways relevant to neuronal functions,
403 such as Ca^{2+} -mediated signaling, Ca^{2+} ion transmembrane transporter activity, synaptic vesicle
404 endocytosis, synaptic transmission, neuronal synaptic plasticity, and synaptic vesicle recycling, were

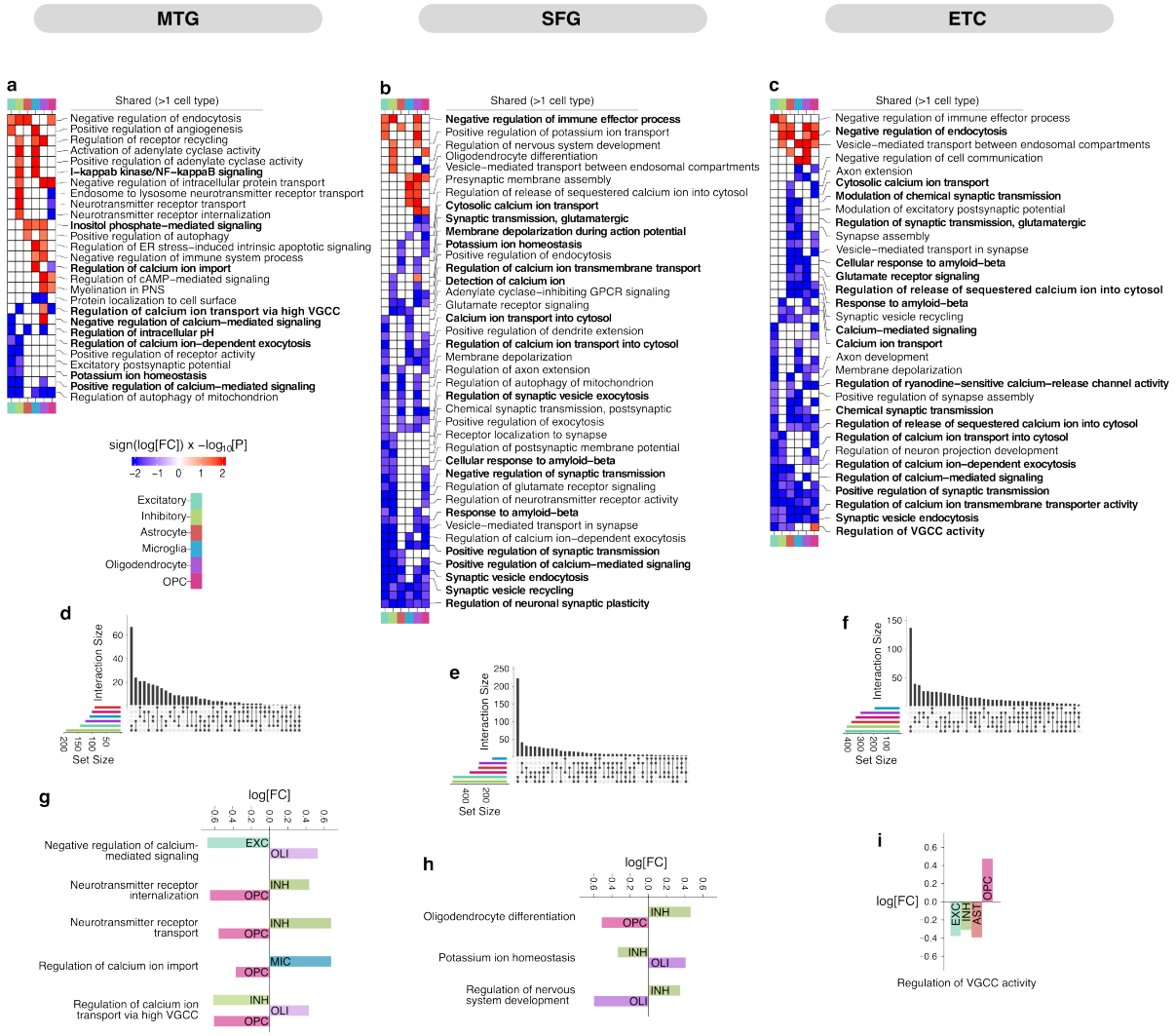

***Figure 3. Broadly dysregulated processes in AD**. (**a—c**). Heatmaps representing select Gene Ontology biological processes dysregulated in more than one cell type (nominal $P < 0.05$). Shared alterations are indicated as evidence of dysregulation in multiple cell types, with red representing upregulation and blue for downregulation. Pathways discussed in the Article are highlighted in bold text. (**d—f**), Upset plots displaying the broadly dysregulated pathways. (**g—i**), Selected pathways exhibiting different dysregulation patterns across cell types.*

consistently downregulated across all cell types in the SFG and ETC (*Fig 3b,c*). These pathways were predominantly downregulated in neurons, indicating that neuronal dysregulation dominates the AD-driven pathway alterations in the SFG and ETC. Concurrently, the observed changes in non-neuronal cell types appear to be closely associated with these neuronal perturbations.

417 To identify consistently perturbed processes across the three brain regions, we assessed the overlap of
418 differentially perturbed pathways in a cell-type-specific manner (*Supplementary Fig. 2; see*
419 *Supplementary Table 12 for full list of overlapping pathways*). We observed considerable concordance
420 of altered cellular process across the three brain regions, with particularly notable overlaps between the
421 SFG and ETC, likely reflective of reduced subject-specific variations. Interestingly, excitatory and
422 inhibitory neurons showed the most pronounced concordance in disrupted processes (*Supplementary*
423 *Fig. 2a*), with 31 pathways in excitatory neurons and 84 pathways in inhibitory neurons showing
424 consistent dysregulations across the three regions. Alterations in inhibitory neurons include consistent
425 downregulation of VGCC activity across all regions, and other key processes like Ca^{2+} -regulated
426 signaling and exocytosis, potassium ion (K^{+}) homeostasis, and neurotransmitter receptor maintenance.
427 Excitatory neurons, on the other hand, consistently expressed disruptions in pathways related to
428 mitochondrial autophagy and Ca^{2+}-dependent exocytosis, underscoring the role of Ca^{2+} signaling in
429 AD-associated cellular perturbations (*Supplementary Fig. 2b*). In contrast, glial cells exhibited less
430 overlap in perturbations, with microglia cells, showing the least concordance. This suggests a broader
431 spectrum of cellular disruptions and region-specific sensitivities to microglial dysregulation in AD.
432 Among the affected processes were intracellular pH regulation, mitochondrial autophagy, and
433 neurotransmitter receptor transport (*Supplementary Fig. 2b*). This variability among glial cells suggests
434 a more complex and region-specific landscape of glial involvement in AD pathology.

435 Together, these findings elucidate the complex nature of cellular responses to AD, demonstrating that
436 the cellular context in which AD manifests leads to markedly divergent molecular perturbations. The
437 observed cell-type and region-specific perturbations highlight the complexity inherent in the regulatory
438 landscape comprising the diverse molecular processes following AD pathogenesis.

439 ***Unraveling AD-associated pathway alterations at systems level***

440 We next ask whether molecular perturbations at the gene level are well represented in the biological
441 processes dysregulated in AD. To accomplish this, we estimated cell-specific differences in gene
442 expression between individuals with AD-pathology and healthy controls (**Methods**) and evaluated the
443 enrichment of DEGs in perturbed processes. Surprisingly, our results reveal that only a small proportion
444 of DEGs across all cell types (*Fig. 4a—c*) were associated with the gene programs (the curated set of
445 genes comprising a biological process) implicated in the perturbed pathways earlier reported (*Fig.*
446 *2&3a—c)*. Notably, among the three brain regions, excitatory neurons in the ETC displayed the most,
447 yet still limited representation, with only 16% of the 3,279 gene programs being DEGs (*Fig. 4d—f*).
448 Neurons consistently showed the most significant degree of DEG representation with a combined 12%
449 overlap in the MTG, 13% in the SFG, and 12% in the ETC. In contrast, astrocytes and microglia
450 demonstrated markedly lower degree of DEG overlap, ranging from 0.5% to 13% across the three
451 regions. These findings illustrate a sparse and varied representation of DEGs within perturbed

452 processes, suggesting that relying solely on DEG analysis may not suffice to capture the full complexity
453 of AD-related molecular changes.

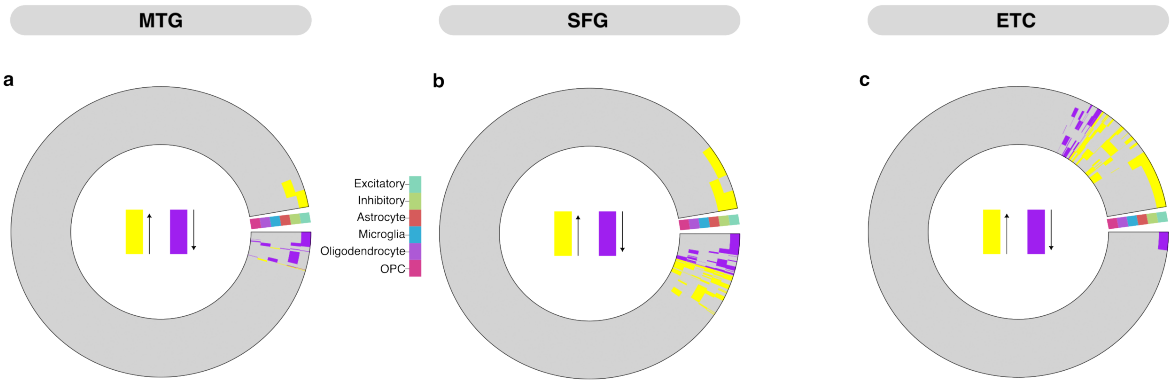

d

	Gene Programs	Up	Down
Excitatory	1218	71	79
Inhibitory	1233	75	76
Astrocyte	946	2	3
Microglia	1544	4	17
Oligodendrocyte	1242	8	17
OPC	848	0	9

e

	Gene Programs	Up	Down
Excitatory	4141	420	185
Inhibitory	3489	318	96
Astrocyte	1594	181	30
Microglia	893	31	4
Oligodendrocyte	1181	118	75
OPC	1741	128	36

f

	Gene Programs	Up	Down
Excitatory	3279	400	136
Inhibitory	2556	113	68
Astrocyte	1513	125	34
Microglia	859	64	4
Oligodendrocyte	1258	118	60
OPC	1575	148	45

454

455 ***Figure 4. DEGs are underrepresented in perturbed gene programs*** *(a—c). Circular heatmaps*
456 *illustrating cell-type specific dysregulation pattern of active genes amongst all perturbed pathways*
457 *(unique and broad). Yellow and purple strips represent upregulated and downregulated genes*
458 *respectively (false discovery rate (FDR) < 0.01 and abs(log_2(fold change)>0.25), while grey regions*
459 *represent non-DEGs, suggesting sparse presence of DEGs relative to total genes within the gene*
460 *programs. (d—f). Table showing number of DEGs in the gene programs comprising perturbed*
461 *pathways in each cell type.*

462

463 Given the sparse and varied distribution of the DEGs within dysregulated processes, we sought to
464 understand the extent to which DEGs influence the AD-associated perturbations at a systems-level. To
465 achieve this, we examined the potential regulatory networks and overarching differences characterizing
466 pathway disruption in AD across all cell types in these brain regions. We interrogated co-expression
467 networks individually for each cell type in each brain region (*Fig 1, 5—8*), identifying groups of genes
468 (gene modules) with high co-expression, suggesting potential co-regulatory mechanism or convergent
469 biological functions. Specifically, network construction was confined to gene programs comprising
470 earlier reported perturbed pathways (*Fig. 2,3)* enabling a fine-grained exploration of the molecular
471 phenotypes governing the complex polygenic perturbations characteristic of AD. Traditional co-
472 expression analysis methods developed for bulk transcriptomic data are not well suited to handle the

473 inherent sparsity and noise in single-cell data (57,58). As a result, inferred networks are prone to
474 spurious gene-gene correlations, thereby complicating the extraction of meaningful systems-level
475 insights (59). To overcome these limitations, we estimate the gene-gene co-expression using
476 hdWGCNA (31), a framework for co-expression network analysis tailored specifically for scRNA-seq
477 data. hdWGCNA accounts for these considerations by aggregating highly similar cells into "metacells",
478 allowing for more accurate co-expression estimations, and facilitating the extraction of meaningful
479 systems-level insights while preserving cellular diversity.

480 ***Neuron-specific co-expression signatures in AD***

481 Using hdWGCNA, we obtained a collection of gene-gene co-expression relationships across neuronal
482 cells in each brain region (*Fig 5&6a—c*). Specifically, in the MTG, we identified 6 distinct excitatory
483 co-expression modules (referred to as EXC-M1 to EXC-M6) (*Fig. 5a*) and inhibitory modules (INH-
484 M1 to INH-M6) (*Fig. 6a*). Since functional insights within a co-expression network often stems from a
485 selected set of nodes possessing high centrality (called hub genes), we reasoned that these hub genes
486 are likely to play pivotal roles in cellular functions due to their extensive network interactions
487 (31,60,61). The network plots highlight the top hub genes within each module, some of which exhibited
488 differential expression (hDEGs, where h indicates that the gene is both a DEG and a hub gene; *see*
489 *Supplementary Table 13 for full list of hub genes*).

490 Strikingly, in the MTG, our results show a concentration of downregulated hDEGs in EXC-M1 (*Fig.*
491 *5a*) and INH-M3 (*Fig. 6a*), primarily associated with cytosolic-localized RNA, such as MT-CO1, MT-
492 ND3, and MT-ATP8. These genes encode essential subunits for oxidative phosphorylation in the
493 electron transport chain, consistent with previous reports highlighting mitochondrial dysfunction,
494 oxidative stress, and impaired cellular metabolism as key processes perturbed during AD pathogenesis
495 (62). Similarly, we identified hDEGs in INH-M4 (*Fig. 6a*) and EXC-M3 (*Fig. 5a*), including members
496 of the calmodulin gene family CALM2 and CALM3, recognized as regulators of intracellular Ca^{2+}
497 signaling, with vital roles in synaptic processes. Previous studies have linked these hub genes to AD
498 (Liu et al., 2020; Morabito et al., 2020; Wang et al., 2010), further substantiating the central role of Ca^{2+}
499 signaling dysregulation in hippocampal AD pathogenesis, in accordance with the Ca^{2+} hypothesis of
500 AD (63,66).

501 Furthermore, additional hDEGs were distributed across three excitatory neuron co-expression modules
502 (EXC-M2, EXC-M5, EXC-M6) (*Fig. 5a*). Among these is the upregulated WASF1 in EXC-M5 (*Fig.*
503 *5a*), with a distinct regulatory role in actin assembly. Notably, downregulation of WASF1 has been
504 linked to substantial reduction of amyloid levels within the hippocampus, indicating a negative feedback
505 mechanism involving the APP intracellular domain—WASF1 pathway (67). The

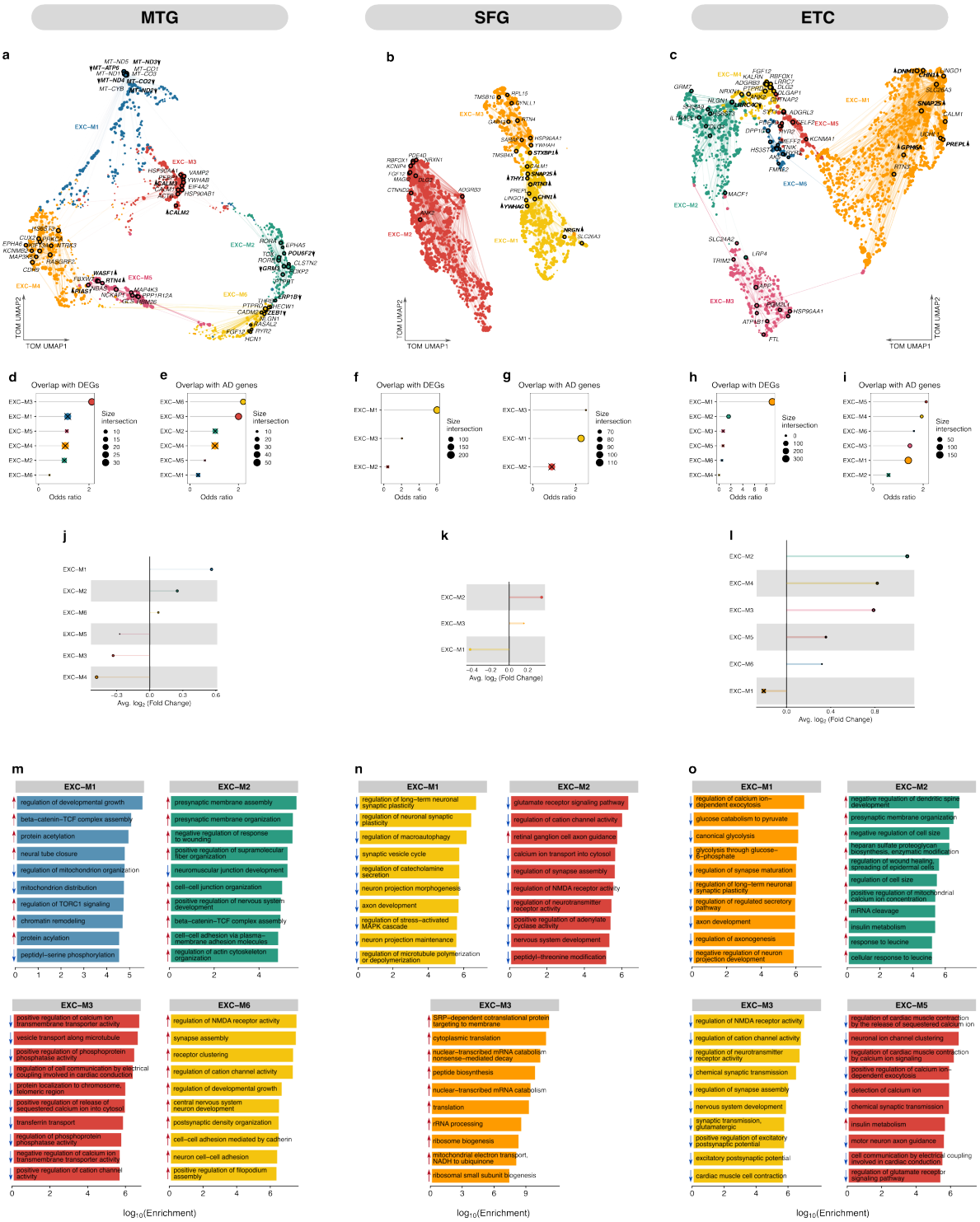

506

507

508 ***Figure 5. Disease-associated gene modules in excitatory neurons using co-expression networks***
509 ***derived from AD-dysregulated gene programs.*** *(a—c). UMAP plot of the topological overlap matrix*
510 *(TOM) illustrating neuronal co-expression networks constructed from genes programs comprising*
511 *dysregulated pathways in excitatory neurons in the (a) MTG, (b) SFG, and (c) ETC. Nodes represent*

*genes, color-coded by module membership, linked by edges depicting co-expression strength, with node size reflecting gene eigengene-based connectivity (**Methods**). Top hub genes are annotated within each module, with bold labels and directional arrows indicating hub-DEGs (hDEGs) as up- or down-regulated. Network visualization is simplified by edge downsampling for clarity. (d—i). Gene overlap analysis showing overlap of DEGs (d, f, h) and AD-associated genes (**Methods**) (e, g, i) with genes within co-expression modules, using Fisher's exact test. An "X" indicates nonsignificant overlap (FDR > 0.05). (j—l). Lollipop plots representing the fold-change of differential expression for Module Eigengenes (DMEs), with the dot size corresponding to the number of genes in the respective module. An "X" overlays modules without statistically significant expression changes (FDR > 0.05). (m—o). Gene Ontology (GO) term enrichment within differentially expressed co-expression modules. Bar plots illustrate the log-scaled enrichment scores; blue arrows indicate downregulated, and red arrows indicate upregulated processes.*

upregulated PIAS1 (EXC-M5), a known modulator of striatal transcription and DNA damage repair during SUMOylation, comprises critical parts of diverse cellular processes associated in neurodegenerative diseases like Huntington's disease, Parkinson's disease, and AD (68). Interestingly, PIAS1 overexpression was found to inhibit several AD marker genes such as NEUROD1, NEUN, MAPK2, GSAP, MAPT, and APP (69). Likewise, the downregulated ZEB1 expressed in EXC-M6 (*Fig. 5a*) underscores the role of transcriptional repression in regulating AD-associated correlations between accessible chromatin peaks and target genes (70). We next interrogated the distribution of DEGs and known AD-related genes using a comprehensive gene compendium from the Open Targets Platform (53), KEGG Alzheimer's disease pathways (54), and Harmonizome (55) (*Fig. 5&6d—i*). Overlap analysis of modules in the MTG (**Methods**) revealed that, while up to 50 DEGs were distributed across excitatory and inhibitory co-expression modules, only EXC-M3 (*Fig. 5a*) exhibited significant enrichment for DEGs (*Fig. 5d*). Notably, three modules—EXC-M3, EXC-M6, and INH-M4—showed significant enrichment for AD-related genes (*Fig. 5&6d,e*). These results underscore the module-specific associations of DEGs and AD-related genes, suggesting intricate and dynamic transcriptional changes within co-expression modules and their potential relevance to AD pathogenesis. Additionally, we identified several AD-related hub genes distributed across excitatory and inhibitory co-expression modules (*Fig. 5&6a*). For instance, hub genes in EXC-M3 (*Fig. 5a*) included AD-associated genes HSP90AA1, HSP90AB1 which have been linked to protein misfolding, chaperoning, autophagy, apoptosis, and stress response—processes central to the dysregulation of protein integrity implicated in AD pathogenesis (71–73). Likewise, the presence of PPP1R12A in EXC-M5 (*Fig. 5a*) highlights its significance in the context of tau hyperphosphorylation and NFT formation, a hallmark of AD (74). Interestingly, EXC-M2 (*Fig. 5a*) expressed RORB, a classical marker of selectively susceptible excitatory neurons (20), while RYR2, expressed in EXC-M6 (*Fig. 5a*), regulates Ca^{2+} homeostasis and

548 neuronal activity, which is central to normal cognitive function (75–77). INH-M4 (*Fig. 6a*) was
549 enriched with key AD-related genes including GAPDH, CLU, and FTH1, involved in oxidative stress,
550 amyloidogenesis, elevated cytotoxicity, and iron dysregulation, processes associated with AD
551 progression. (78–81). Similarly, INH-M6 (*Fig. 6a*) contained DPP10, known to influence K^+ channel
552 activity and exhibit pronounced reactivity in the vicinity of NFTs and plaque-associated dystrophic
553 neurites (82).

554 Next, we compared system-level differences in gene expression between AD and control groups using
555 differential module eigengene (DME) analysis (**Methods**) (*Fig. 5&6 j—l*) (31). DME analysis of MTG
556 derived neuronal modules revealed marked differences in the magnitude and direction of module
557 expression from control to AD (*Fig. 5&6j*) (Wilcoxon rank-sum test Bonferroni-adjusted $p < 0.05$;
558 Supplementary Tables 9—11). These results suggest that AD-induced alterations in systems-level gene
559 expression changes reflect either an enhancement of or decline in the functionality of co-regulated gene
560 networks (83,84). Interestingly, all four down-regulated modules (*Fig. 5&6j*) (EXC-M3, EXC-M4,
561 EXC-M5, INH-M4), exclusively comprised downregulated hDEGs (*Fig. 5&6a*). Conversely,
562 upregulated modules (*Fig. 5&6j*) solely contained upregulated hDEGs (*Fig. 5&6a*), suggesting a pivotal
563 role for hDEGs in perturbation of co-expression networks that characterize AD-related biological
564 processes. Unsurprisingly, the downregulated excitatory module, EXC-M1, (*Fig. 5j*), enriched for
565 mitochondrial-related hDEGs (*Fig. 5a*), was distinctively associated with differentially expressed
566 pathways pivotal for numerous cellular processes and developmental functions (*Fig. 5m*). These
567 include the regulation of development, assembly of the beta-catenin-TCF complex, protein acetylation,
568 neural tube closure, mitochondrial organization and distribution, TORC1 signaling, chromatin
569 alterations, protein acylation, and peptidyl-serine phosphorylation (*Fig. 5m*). Similarly, INH-M3 (*Fig.*
570 *5a*) was associated with genes that contribute to RNA processing, energy synthesis and metabolism,
571 and protein stability (*Fig. 6m*) and was upregulated in AD (*Fig. 6j*). Moreover, other dysregulated
572 modules (*Fig. 5&6i*) were found to be enriched for genes associated with a variety of biological
573 processes crucial for normal neuronal functions, including synapse assembly (EXC-M2 & EXC-M6),
574 vesicle transport (EXC-M3, EXC-M4, EXC- EXC-M7, EXC-M10, EXC-M13), Ca^{2+} transmembrane
575 transport (EXC-M3, INH-M4), and synaptic vesicle exocytosis (INH-M2), which have been previously
576 implicated in AD pathophysiology (*Fig. 5&6m*).

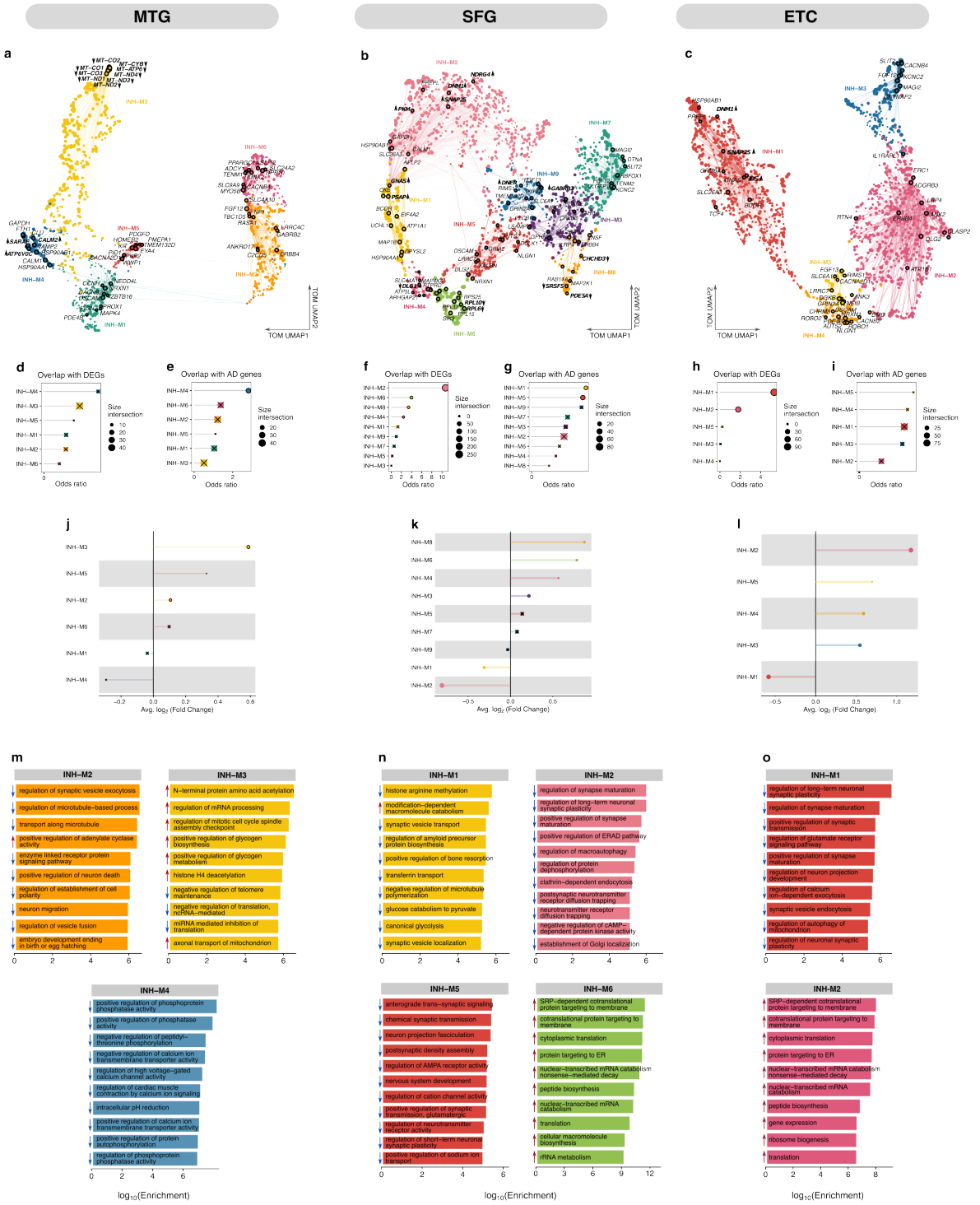

577

578 ***Figure 6. Disease-associated gene modules in inhibitory neurons using co-expression networks***
579 ***derived from AD-dysregulated gene programs***. *(a—c). UMAP plot of the TOM illustrating neuronal*
580 *co-expression networks constructed from genes programs comprising dysregulated pathways in*
581 *inhibitory neurons in the (a) MTG, (b) SFG, and (c) ETC. Nodes represent genes, color-coded by*
582 *module membership, linked by edges depicting co-expression strength, with node size reflecting gene*
583 *eigengene-based connectivity (see Methods). Top hub genes are annotated within each module, with*

584 *bold labels and directional arrows indicating hDEGs as up- or down-regulated. Network visualization*
585 *is simplified by edge downsampling for clarity. (d—i). Gene overlap analysis showing overlap of DEGs*
586 *(d, f, h) and AD-associated genes (**Methods**) (e, g, i) with genes within co-expression modules, using*
587 *Fisher's exact test. An "X" indicates nonsignificant overlap (FDR > 0.05). (j—l). Lollipop plots*
588 *representing the fold-change of DMEs, with the dot size corresponding to the number of genes in the*
589 *respective module. An "X" overlays modules without statistically significant expression changes (FDR*
590 *> 0.05). (m—o). GO term enrichment within differentially expressed co-expression modules. Bar plots*
591 *illustrate the log-scaled enrichment scores; blue arrows indicate downregulated, and red arrows*
592 *indicate upregulated processes.*

593

594 Co-expression analysis of neuronal cells in the SFG, resulted in a total of 12 excitatory and inhibitory
595 modules (*Fig. 5b&6b*). Interestingly, EXC-M1 and M3 were significantly enriched in AD-associated
596 genes and DEGs (*Fig. 5f,g*). Consistent with our observations in the MTG, AD-related hDEGs in the
597 downregulated EXC-M1 (*Fig. 5k*), include SNAP25, NRGN**,** THY1, and RTN3, which are implicated
598 in various processes central to AD pathophysiology, including synaptic neurotransmission, synaptic
599 plasticity, synaptic signaling, immune response, neuron development, and endoplasmic reticulum (ER)
600 morphology and function (*Fig. 5n*). Moreover, EXC-M2, though upregulated in AD (*Fig. 5k*), was
601 associated with synaptic function, neuronal development, and signal transduction (*Fig. 5n*). A hub gene
602 identified in EXC-M2, PDE4D, has been previously shown to result in abnormalities in the topological
603 organization of functional brain networks (85). As a phosphodiesterase, PDE4D plays a pivotal role in
604 regulating cAMP dynamics in neurons and glial cells (86), which ultimately influence memory
605 formation and neuroinflammation (85,87). We noted GAP43, expressed in EXC-M3, whose elevated
606 expression is recognized as a marker for tau and amyloid-driven pathologies. GAP43 also has a
607 significant role in neural cell development, axonal sprouting, and regeneration (88–90). We also found
608 enrichment of other AD-associated genes that have been prioritized as target genes in AD such as
609 LINGO1 (EXC-M1) (91), NRGN (EXC-M1) (92), ADGRB3 (EXC-M2) (93), and RTN4 (EXC-M3)
610 (94). This supports the notion that hub genes in these co-expression modules of the SFG are indicative
611 markers of pathway dysregulation in excitatory cells in AD.

612 A total of 6 inhibitory modules were significantly enriched for DEGs or AD-related genes (*Fig. 6f,g*).
613 In contrast to our observation in excitatory cells (*Fig. 5f,g*), none of these modules displayed
614 simultaneous enrichment for both DEGs and AD-related genes (*Fig. 6f,g*). We observed a consistent
615 pattern—either upregulation or downregulation—in the directionality of the hDEGs within their
616 respective modules (INH-M1, INH-M2, INH-M4, INH-M6, INH-M8, and INH-M9) (*Fig 6b*).
617 Surprisingly, and contrary to observations in the MTG (*Fig. 5&6a*), all hDEGs in both excitatory and
618 inhibitory networks were counter-directional to the differentially expressed module eigengenes (DMEs)

619 (*Fig. 5&6b*). This finding emphasizes the central role of hDEGs in the dysregulation of co-expression
620 networks within AD-related pathways and suggests a robust region-specific association between
621 hDEGs and module dysregulation. Notably, upregulated hDEGs such as SNAP25 and DNM1 in the
622 INH-M2 (*Fig. 6b*), play critical roles in regulating synaptic vesicle fusion and recycling (95,96). Also,
623 PKM, which is upregulated in INH-M1 (*Fig. 6b*) and is involved in glycolysis, is associated with
624 aberration role in the regulation of metabolism and synaptic function in AD (*Fig. 6n*) (97–99).
625 Moreover, the presence of upregulated PSAP in INH-M1 (*Fig. 6b*), underscores its role in lysosomal
626 catabolism of glycosphingolipids (*Fig. 6n*) (100), and further highlights its significance in lysosomal
627 dysfunction and neuronal survival in AD (101). We also observed enrichment of other key AD-related
628 hub genes, particularly those regulating synaptic function in INH-M5 and INH-M4 (*Fig. 6b,n*). These
629 include DLG1, a hDEG in INH-M4, DLG2, GRIA2, NLGN1, and NRXN1, in INH-M5 (102). Similar
630 to the enrichment of RNA processing observed in EXC-M3, we detected a significant presence of
631 ribosomal related genes in INH-M6, notably the downregulated hDEGs RPL6 and RPL10 (*Fig. 6b,n*).
632 These genes are critical for protein synthesis and have been linked to regulation of metal ion
633 homeostasis and cell death in AD (102–104).

634 Interestingly, we observed a recurring theme in the neuronal co-expression networks in the ETC (*Fig.*
635 *5&6c)*. hDEGs identified in the SFG, including SNAP25, DNM1, CHN1, and DNM1 were also found
636 to be hDEGs in EXC-M1 and INH-M1 in the ETC (*Fig. 5&6c*). In the same vein, all hDEGs across
637 EXC-M1 and INH-M1 exhibited opposing directionality compared to the DMEs (*Fig. 5&6c,l*).
638 Additionally, other AD-related hub genes were found to be shared across excitatory modules in both
639 brain regions (*Fig. 5b,c*). These genes, including GRIN2A, NLGN1, NRXN1, and SLC6A1, play
640 critical roles in synaptic formation, function, signaling, and plasticity. Notably, the heat shock protein
641 HSP90AB1, essential for protein folding, was also identified as an AD-related hub gene shared among
642 the excitatory modules. Similarly, we identified shared inhibitory hub genes with relevance to AD, such
643 as CALM1, HSP90AA1, PDE4D, NRXN1, and RTN3. These genes assume particular significance in
644 the perturbation of biological processes in AD due to their involvement in Ca^{2+} signaling, tau pathology,
645 synaptic function, cAMP modulation, protein aggregation, and neurotransmission. Furthermore,
646 analysis of DME patterns across the three brain regions revealed a unique relationship between gene
647 co-expression modules and associated pathways (*Fig. 5&6j—o*). Remarkably, dysregulated modules
648 exhibited a predominant enrichment for pathways perturbed in a specific direction. For instance, across
649 excitatory and inhibitory modules in the ETC, the top enriched pathways were either consistently
650 downregulated (EXC-M1, EXC-M3, and INH-M1), consistently upregulated (EXC-M2 and INH-M2),
651 or predominantly downregulated (EXC-M5) (*Fig. 5&6o*). Interestingly, while certain DMEs displayed
652 opposing dysregulation patterns relative to their corresponding enriched pathways, others demonstrated
653 concordant dysregulation with enriched processes (*Fig. 5&6j—o*).

654 Taken together, these findings highlight the centrality of hDEGs and other AD-associated hub genes in
655 orchestrating neuronal perturbations underlying the biological processes disrupted in AD. Hub genes
656 identified within these networks shed light on the mechanisms of synaptic function, protein folding, and
657 signaling that are significantly perturbed in neurons in AD. Furthermore, the alignment between
658 dysregulated modules, enriched pathways, and hDEGs reinforces the notion of AD as a systems disease,
659 characterized by tightly linked alterations in gene networks and their associated functional pathways.

660 ***Glial-specific co-expression signatures in AD***

661 To conceptualize the AD-driven systems-level perturbations in glial cells, we next probed the astrocyte
662 (AST-M) and microglia (MIC-M) co-expression modules (*Fig. 7&8*). Contrary to the previously
663 characterized neuronal co-expression patterns in the MTG (*Fig. 5&6d,e*), we observe that only one glial
664 module, MIC-M5 (*Fig. 8a*), displayed significant enrichment for DEGs, and notably, was the only
665 module containing hDEGs (*Fig. 7a,b,c,f,g,h*). This suggests a potentially limited role of DEGs in
666 orchestrating systems-level differences in glial cells. While all astrocyte and microglia modules that
667 displayed significant dysregulation in AD (*Fig. 7&8j*), contain AD-related hub genes (*Fig. 7&8a*), only
668 AST-M3 and AST-M1 were predominantly enriched for AD-associated genes (*Fig. 7e*). Specifically,
669 AST-M1, upregulated in AD (*Fig. 7i*), contained critical hub genes such as the glial high-affinity
670 glutamate transporter, SLC1A2, a gene linked to altered glutamate homeostasis in AD and fundamental
671 for preventing excitotoxicity in astrocytes and neurons (105,106); SLC4A4, a key regulator of neuronal
672 pH homeostasis; and others including GPM6A, STXBP5, CACNB2, and ERBB4, which play roles in
673 neurodevelopment, synaptic function and plasticity (107–111). Furthermore, AST-M2, which was
674 upregulated in AD, contained hub genes linked to processes such as intracellular protein recycling
675 (RAB11FIP3), immune response regulation, neuronal development, synaptic plasticity (IL1RAPL1,
676 PTPRD), synaptic vesicle release (RIMS2, SYT1), and Ca^{2+} signaling (RYR2) (*Fig. 7a*). Conversely,
677 the downregulated astrocyte module M3 (*Fig. 7j*) was enriched for stress-response genes including heat-
678 shock genes (HSPA1A, HSPA1B), and genes critical for extracellular matrix organization and cellular
679 adhesion (VCAN, CD44) (*Fig. 7a*).

680 Remarkably, hub genes in MIC-M2 included classical markers of DAM, such as APOE, B2M, CST3,
681 and CD81, along with genes involved in RNA and ribosomal processing (RPS27A, RPS15, RPS19, and
682 RPS28) (*Fig. 8a*). This supports the notion that system-level upregulation observed in MIC-M2 is linked
683 to the dysregulated immune response and activation of phagocytic states in microglia. Indeed MIC-M2
684 displayed enrichment for processes related to microglial inflammatory activation, including pathways

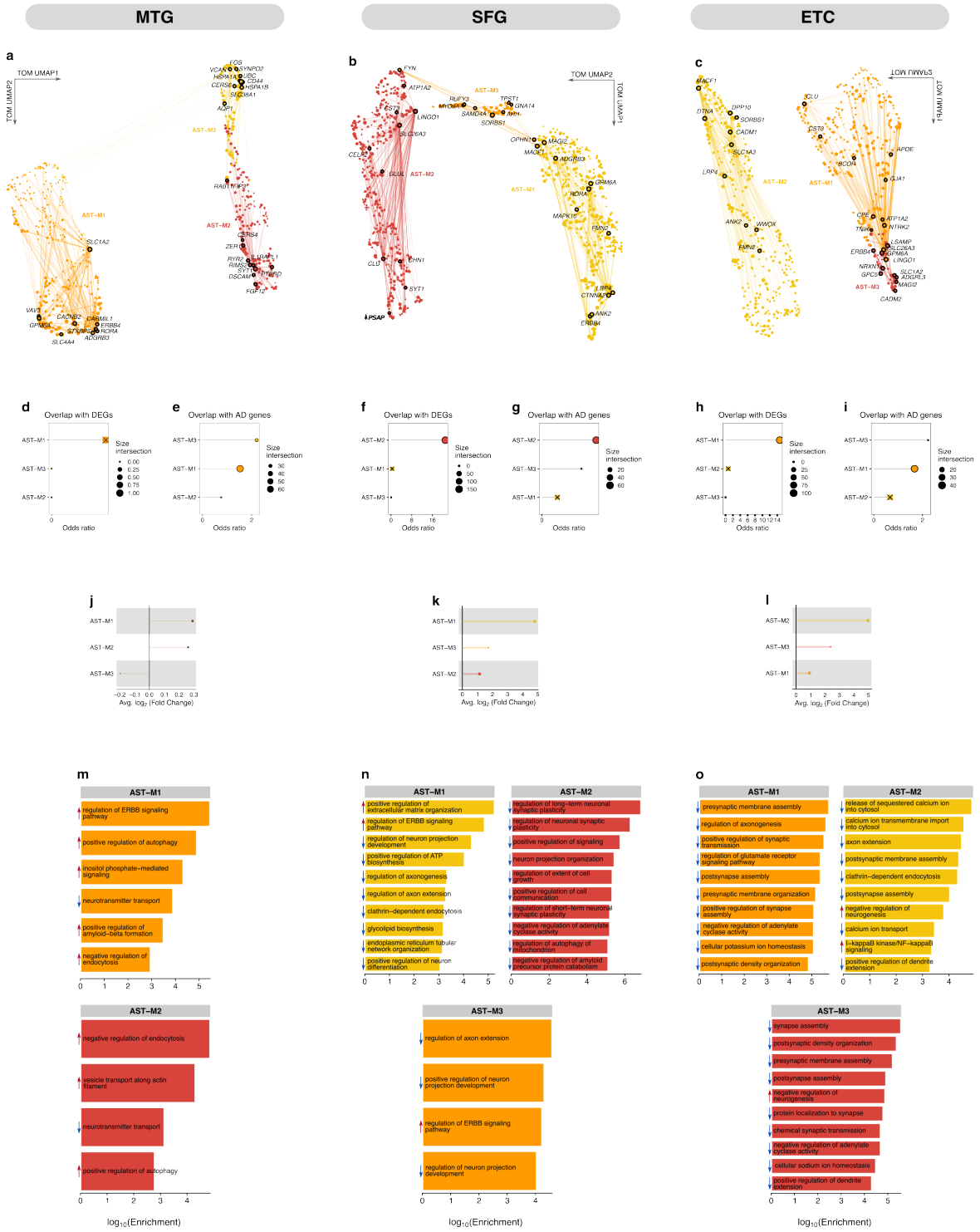

Figure 7. Disease-associated gene modules in astrocytes using co-expression networks derived from AD-dysregulated gene programs. *(a—c). UMAP plot of the TOM illustrating glial co-expression networks constructed from genes programs comprising dysregulated pathways in astrocytes in the (a) MTG, (b) SFG, and (c) ETC. Nodes represent genes, color-coded by module membership, linked by edges depicting co-expression strength, with node size reflecting gene eigengene-based connectivity*

*(see Methods). Top hub genes are annotated within each module, with bold labels and directional arrows indicating hDEGs as up- or down-regulated. Network visualization is simplified by edge downsampling for clarity. (d—i). Gene overlap analysis showing overlap of DEGs (d, f, h) and AD-associated genes (**Methods**) (e, g, i) with genes within co-expression modules, using Fisher's exact test. An "X" indicates nonsignificant overlap (FDR > 0.05). (j—l). Lollipop plots representing the fold-change of DMEs, with the dot size corresponding to the number of genes in the respective module. An "X" overlays modules without statistically significant expression changes (FDR > 0.05). (m—o). GO term enrichment within differentially expressed co-expression modules. Bar plots illustrate the log-scaled enrichment scores; blue arrows indicate downregulated, and red arrows indicate upregulated processes.*

like I−kappaB kinase/NF−kappaB signaling, ER stress response regulation, and ER−induced apoptotic signaling, along with modulation of adenylate cyclase activity and mitochondria autophagy (*Fig. 8m*). Similarly, hub genes in MIC-M5 were primarily associated with lipid processing and immune response (*Fig. 8a*). These included genes such as GPNMB, LRRK2, MITF, ABCA1, STARD13, ZBTB16, and PRKAG2. Notably, GPNMB, a critical regulator of microglial activation and neuroinflammation, has been demonstrated to stimulate the production of pro-inflammatory cytokines, thus contributing to the inflammatory cascade observed in AD (112–115). Further reinforcing the activated state of microglia, MIC-M4 contained critical hub genes like PICALM, which governs clathrin-mediated endocytosis and is fundamental to Aβ clearance (116,117); DOKC2, a key regulator of Rho GTPase activation, which are essential components in immune cell trafficking and microglial mobility (118,119); and TAB2, a multi-functional adaptor protein involved in multiple cellular stress response pathways including TGF-beta and NF-kappaB signaling. Conversely, MIC-M3 and MIC-M1 were significantly downregulated (*Fig. 8j*) in AD and contained hub genes involved with protein folding, stress response, intracellular signaling, signal transduction, and synaptic function (*Fig. 8a,m*). Particularly, NLGN1 in MIC-M1, which is critical for the formation and maintenance of synapses, emphasizes the role of microglia in synaptic pruning and modulating neuronal connectivity. Additionally, the presence of RYR2 and PLCB1 in MIC-M1 suggests a crucial role for Ca^{2+} -mediated signaling pathways in modulating neuroinflammation and phagocytic activity of microglia.

Co-expression analysis of astrocyte and microglial gene programs in the SFG revealed 6 distinct modules (*Fig. 7&8a*). Strikingly, DME analysis revealed that all astrocyte and microglia modules are downregulated in AD (*Fig. 7&8k*), consistent with the predominant pattern of pathway downregulation observed in SFG (*Fig. 2e*).

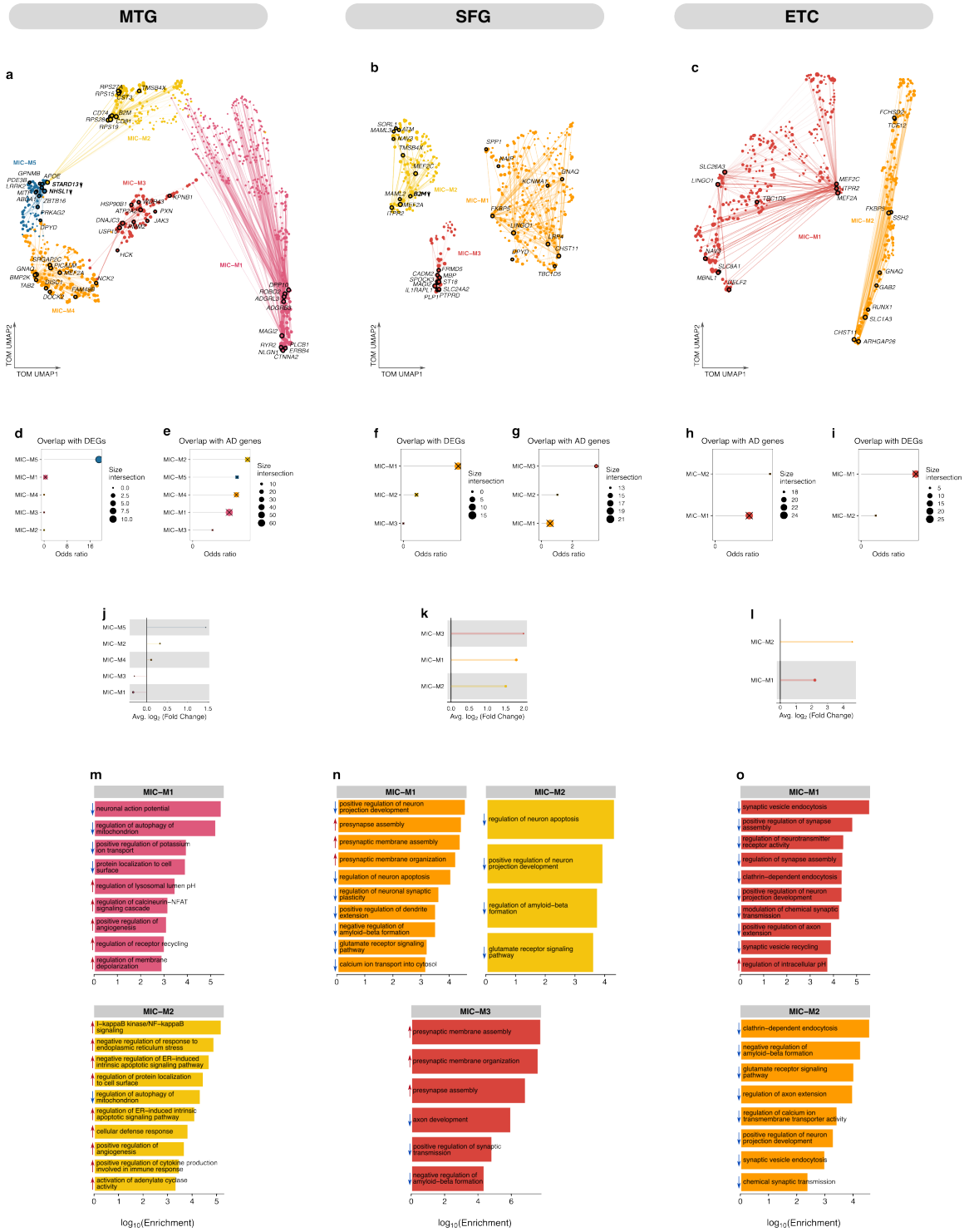

723

724 ***Figure 8. Disease-associated gene modules in microglia using co-expression networks derived from***
725 ***AD-dysregulated gene programs***. *(a—c). UMAP plot of the TOM illustrating glial co-expression*
726 *networks constructed from genes programs comprising dysregulated pathways in microglia in the (a)*
727 *MTG, (b) SFG, and (c) ETC. Nodes represent genes, color-coded by module membership, linked by*

*edges depicting co-expression strength, with node size reflecting gene eigengene-based connectivity (**Methods**). Top hub genes are annotated within each module, with bold labels and directional arrows indicating hDEGs as up- or down-regulated. Network visualization is simplified by edge downsampling for clarity. (d—i). Gene overlap analysis showing overlap of DEGs (d, f, h) and AD-associated genes (Methods) (e, g, i) with genes within co-expression modules, using Fisher's exact test. An "X" indicates nonsignificant overlap (FDR > 0.05). (j—l). GO term enrichment within differentially expressed co-expression modules. Bar plots illustrate the log-scaled enrichment scores; blue arrows indicate downregulated, and red arrows indicate upregulated processes. (m—o). Lollipop plots representing the fold-change of DMEs, with the dot size corresponding to the number of genes in the respective module. An "X" overlays modules without statistically significant expression changes (FDR > 0.05).*

This reinforces the link between gene co-expression networks and the orchestration of functional perturbations of biological processes in AD. Surprisingly, AST-M2 emerged as the only module exhibiting significant enrichment for AD-associated genes and DEGs (*Fig. 7&8f,g*), implying a critical role for AST-M2 in orchestrating astrocytic function in the context of AD. Specifically, AST-M2 contained several AD-associated hub genes with distinct functional relevance. For instance, SYT1, a key regulator of synaptic vesicle exocytosis and neurotransmitter release (120), and LINGO1 associated with the perturbation of neural growth and AD-associated myelination defects in AD (91), are hub genes in AST-M2. In addition, ATP1A2, a gene essential for astrocytic regulation of neuronal excitability via the maintenance of \ K^+ and Na^+ homeostasis (121), was also identified as a hub gene in this module. Other hub genes included GLUL, essential for astrocytic clearance of synaptic glutamate (122), and PSAP, an upregulated hDEG, implicated in dysregulation of lysosomal function and lipid metabolism in AD (101,123). Notably, classical markers of reactive disease associate astrocytes (DAA), CST3 and CLU, were also hub genes in AST-M2, known for their involvement in the clearance and accumulation of Aβ (26). Indeed, GO term enrichment revealed a robust array of biological processes governed by AST-M2, including maintenance of synaptic plasticity, signaling cascades, neuronal growth and repair, intercellular communication, and Aβ aggregation and clearance (*Fig. 7n*). This spectrum of functions effectively contextualizes the role of AST-M2 in the astrocyte-mediated maintenance of synaptic function and overall neuronal health, thus highlighting the integral role of neuron-glial crosstalk in the perturbation of the functional dynamics underpinning AD-related processes (124–126). We also found enrichment of genes associated with synaptic organization, cellular communication, energy metabolism, and development of neural structures in AST-M1 and AST-M3 (*Fig. 7b*). Indeed, hub genes in these modules play crucial roles in AD-associated process, including FYN in AST-M3, implicated in abnormal phosphorylation of tau protein and mediation of Aβ toxicity (127,128). Additionally, MAPK10, a hub gene in AST-M1, is essential for signaling pathways that regulate various cellular processes, including synaptic plasticity, neuronal survival, and apoptosis (129–131).

764 Consistent with our findings in the MTG, the microglial networks in the SFG also contained hub genes
765 involved in a variety of processes relevant to both AD and microglial activation (*Fig. 8b*). Hub genes
766 in MIC-M1 included SPP1, NAIP, LINGO1, LRP4, TBC1D5, reflecting the enrichment for immune
767 response, synaptic maintenance, and overall neuronal function (*Fig. 8b,n*). Notably, SPP in MIC-M1 is
768 integral for the regulation of phagocytic markers, thus playing a vital role in synaptic engulfment in the
769 presence of Aβ (132). Also involved in the regulation of autophagy is TBC1D5, a hub gene in MIC-
770 M1, functioning as a molecular switch for membrane trafficking between endosomal and
771 autophagosomal pathways (133). MIC-M2 featured hub genes SORL1 and B2M, both implicated in a
772 variety of AD-related processes such as trafficking of APP and resultant amyloidosis in AD (134–138).
773 These genes further underscore the role of endolysosomal—autophagic network in regulating
774 microglial activation (139). Additionally, MIC-M3 displayed enrichment for processes including
775 synaptic assembly and axon development, consistent with the presence of hub genes MBP, PLP1, and
776 PTPRD. This observation also underscores the notion that microglia, while often characterized
777 primarily by their role in immune response in AD, also engage an array of processes vital for
778 maintaining neuronal integrity, such as neural development, synaptic organization, myelin formation
779 and maintenance.

780 Glial co-expression patterns in ETC are similar to those observed in the SFG (*Fig. 7&8c*). Remarkably,
781 all astrocytic and microglial modules in the ETC exhibited downregulation in AD (*Fig. 7&8l*) and were
782 mostly enriched for downregulated pathways (*Fig. 7&8o*), reinforcing the prevailing theme of pathway
783 downregulation witnessed in the ETC (*Fig. 2e*). AST-M1 in the ETC exhibited considerable
784 concordance with AST-M2 in the SFG, with hub genes CLU, CST3, and APOE, reflecting the DAA
785 signature (*Fig. 7c*). However, no microglia module showed significant enrichment for hub genes
786 signaling activated microglia state (*Fig. 8c*). AST-M1 remained the only module demonstrating
787 significant enrichment for both DEGs and AD-related genes (*Fig. 7h,i*). Consistent with previous
788 observation in the SFG, this highlights a pivotal role for the observed co-expression patterns in
789 regulating astrocytic functions in the context of AD. Additional astrocyte hub genes in the ETC,
790 including NRXN1, CADM1, MACF1, MAGI2, LRP4, GJA1 and ADGRL3, have been identified as
791 markers of a reactive astrocyte state, implicating them in amyloidosis, regulation of neuroinflammation,
792 cellular interactions (Dai et al., 2023). Notably, cellular adhesion hub genes, CADMI and NRXN1, have
793 been previously noted as critical for maintaining the synaptic integrity and are hypothesized to
794 contribute to excitotoxicity by impairing the function of reactive astrocytes in the regulation of
795 extracellular ion balance, pH, and glutamate concentration (141–143). We also identified a compelling
796 cross-regional consistency with the identification of shared hub genes—ANK2, ATP1A2, CLU, CST3,
797 ERBB4, FMN2, GPM6A, LINGO1, LRP4, MACF1, MAGI2, SLC26A3, and SORBS1—between the
798 ETC and SFG modules (*Fig. 7b,c*). Given the data for both regions were obtained from the same cohort,
799 these hub genes emerge as potential brain-wide markers for astrocytic reactivity in AD. Likewise,

800 shared microglia hub genes include CHST11, FKBP5, GNAQ, ITPR2, LINGO1, MEF2A, MEF2C,
801 NAV3, and TBC1D5 (*Fig. 8b,c*), revealing complex interplay of functional involvements, including
802 extracellular matrix modification, G-protein signaling, and intracellular Ca^{2+} regulation.

803 These results provide a robust systems-level perspective on the functional diversity within astrocyte
804 and microglial modules in AD. We identified specific modules in these glial cell types that exhibit
805 perturbations and are enriched for glial-specific processes and hub genes, yet notably did not
806 prominently feature hDEGs. This suggests that the pathophysiological mechanisms in astrocyte and
807 microglia may rely more on the dysregulation of gene networks and associated pathways rather than
808 isolated gene perturbations. For instance, microglial modules, such as MIC-M2 and MIC-M4 in the
809 MTG, primarily feature non-DEGs linked to DAM activation and microglial inflammatory responses.
810 This is complimented by the functional downregulation observed in MIC-M3 and MIC-M1, which,
811 despite a lack of enrichment for DEGs, feature genes crucial for protein folding, cellular stress response,
812 and synaptic maintenance. Likewise, astrocyte modules, though not enriched with hub-DEGs, display
813 a spectrum of AD-related alterations peculiar to astrocytic functions, from glutamate homeostasis to
814 intracellular protein recycling and stress response. Together, our results offer a robust framework for
815 appreciating the role of genes in glial alterations associated with AD, extending beyond differential
816 gene expression profiles to the broader systems-level interplay of gene interactions underpinning AD
817 pathogenesis.

818 ***Conserved molecular drivers underlying pathway dysregulation***

819 Our analysis reveals pronounced modular heterogeneity and extensive functional disruptions in neurons
820 and glia across the brain regions. To further identify potential common drivers directing these pathway
821 perturbations across regions, we examined recurrent hub genes within each cell type (Supplementary
822 Table 14). Excitatory neurons showed substantial overlap of hub genes mostly participating in Ca^{2+}
823 regulation, autophagy, proteostasis, cell-cell adhesion, neuronal cell death, and synapse regulation.
824 Notably, most of these hub genes were non-DEGs in at least one brain region yet are AD-related and
825 co-expressed in similar modules across all three regions. This further reinforces the notion that
826 coordinated dysregulation of genes within a module, rather than changes in select individual genes, may
827 promote pathway perturbations. Particularly, 6 hub genes—ACTB, CALM1, CALM2, GAPDH,
828 HSP90AB1, and UCHL1—consistently belong to the same module in each brain region. Given their
829 known roles in Ca^{2+} signaling, protein homeostasis, and neuronal apoptosis, these genes likely serve as
830 region-wide orchestrators directing alterations in neuronal pathways fundamental for normal function.
831 Inhibitory neurons demonstrated comparable overlap of non-differentially expressed hub genes
832 participating in Ca^{2+}-mediated signaling and synaptic transmission. As with excitatory neurons, the
833 majority of these hub genes are AD-related and co-expressed in the same module, including CALM1,

HSP90AA1, PDE4D, and NRXN1. Their function in regulating critical neuronal processes likely positions them as potential conserved mediators of pathway disruptions.

Among glial cells, microglia exhibited the highest hub gene overlap consisting of GNAQ, MAML3, MEF2A, MTHFD1L, and TGFBR1. These genes govern an array of processes critical for microglial activation, including inflammation, immune responses, and signaling cascades, potentially indicating conserved mechanisms underlying microglial reactivity across brain regions affected in AD. Likewise, the only overlapping astrocytic hub genes, ERBB4 and GPM6A, assume extensive roles in pathways related to neuroinflammation and synaptic dysfunction.

Overall, our analysis of recurrent hub genes points to potential conserved orchestrators of pathway disruptions across brain regions in AD. Experimental validation of these predictions remains vital to firmly establishing their functional significance. Nonetheless, our multi-region analysis provides a foundation to guide future investigations into common mechanisms directing AD pathogenesis.

Discussion

Here, we leverage pathway activity and gene co-expression analyses to delineate the complex, systems-level alterations that characterize AD neuropathology. While scRNA-seq has been pivotal in revealing the molecular signatures of AD, much emphasis has been placed on differentially expressed genes without a comprehensive examination of the role and functional interconnectivity among these genes in biological processes across brain regions and cell types. This limitation largely renders associated studies insufficient for capturing the complexity of AD as a systems disease. Utilizing snRNA-seq data profiled from postmortem brain samples of the middle temporal gyrus, superior frontal gyrus, and entorhinal cortex, we reveal an intricate dynamics of perturbed gene networks underpinning the pathology in both neuronal and glial cell types.

The pathophysiological landscape of AD is distinctly marked by cellular and regional heterogeneity, as demonstrated in this study. In the MTG, for instance, AD-induced dysregulations in synaptic functions were significantly more prevalent in neurons compared to glial cells, corroborating previous findings that implicate synaptic dysfunction as a key pathological feature of AD (10). Additionally, our observations of unique pathway dysregulations in glial cells in the MTG contribute to the emerging discourse on the role of glial cells in mediating synaptic impairment in AD etiology (144–146). In the SFG and ETC, we detect a broad downregulation of molecular pathways across multiple cell types, suggesting a more advanced and pervasive pathological state. This is consistent with the known sequential propagation of AD-related pathology across different brain regions (147,148). Interestingly, Ca^{2+} signaling emerged as a shared hub of dysregulation but manifests variably among cell types and regions, underlining opportunities for cell type- and region-specific interventions. This is of

868 considerable interest as Ca^{2+} homeostasis is critical for various cellular functions and its disruption has
869 been considered central to AD pathogenesis (63). We argue that such cellular and regional specificity
870 could not only serve as unique biomarkers for disease states but may also be exploited for targeted drug
871 development.

872 A critical observation in our study is the limited distribution of DEGs among the gene programs
873 comprising the perturbed pathways. This underscores the limitation and inadequacy of conventional
874 pathway analyses or DEG-centric approaches in fully elucidating the complex systems-level alterations
875 characteristic of AD. Thus, our work here expands upon traditional differential expression analyses to
876 capture intricate interplay within gene co-expression networks. As a result, we delineate AD-related
877 hub genes within enriched co-expression modules, implicating a range of biological processes from
878 cellular metabolism to oxidative stress and Ca^{2+} homeostasis. Such an expansive approach broadens the
879 spectrum of putative therapeutic targets and underscores the necessity for systems-level intervention
880 strategies. Importantly, our results demonstrate that AD inflicts a broad spectrum of functional
881 perturbations of gene co-expression across the three brain regions. This heterogeneity in modular
882 responses provides compelling evidence that AD represents collective molecular perturbations,
883 encompassing a spectrum of disruptions across neuronal and glial cells. Notably, we identify distinct
884 patterns of hub-DEGs in specific modules, with a predominant distribution in both excitatory and
885 inhibitory modules, but markedly less presence in glial modules. This pattern suggests that while DEGs
886 have a substantial impact on neuronal cells in the context of AD, their influence on glial cells appears
887 more limited. Given the propensity of co-expression networks to operate as integrated biological units,
888 these findings lend support to the hypothesis that DEGs exert a disproportionately significant impact
889 on neuronal dysfunction vis-à-vis the broader systems-level perturbations characteristic of AD.

890 Our study revealed a significant degree of functional heterogeneity among identified hDEGs. For
891 instance, the upregulated hDEGs, WASF1 and PIAS1 are associated with actin assembly and DNA
892 repair, respectively—mechanisms previously implicated in various neurodegenerative conditions,
893 including AD (67,68). Additionally, the downregulated ZEB1 points to the role of epigenetic
894 modifications, like accessible chromatin peaks, in AD pathology (70). We also identified certain
895 modules particularly enriched for known AD-related genes, highlighting module-specific correlations
896 with AD-driven pathway alterations. Hub genes in these enriched modules, including HSP90AA1 and
897 HSP90AB1, GAPDH, CLU, and FTH1, implies a complexity that may signify both causative and
898 reactive changes in AD pathogenesis. Moreso, our analysis revealed a prominent theme of
899 mitochondrial dysfunction, underscored by the downregulation of hDEGs such as MT-CO1, MT-ND3,
900 and MT-ATP8 in neuronal modules. The presence of these hDEGs lends compelling credence to the
901 hypothesis that aberrations in mitochondrial dysfunction, cellular metabolism, and oxidative stress are
902 key features of the AD pathological cascade (62). We also observed key hDEGs belonging to the
903 calmodulin gene family (CALM2 and CALM3) in neuronal modules. Given the well-established role

904 of these genes in regulating intracellular Ca^{2+} signaling, this observation adds a new perspective to the
905 Ca^{2+} hypothesis of AD and is consistent with earlier works implicating them in disrupted Ca^{2+} signaling
906 (13,63–66).

907 Differential module eigengene analysis further reinforced the notion that AD-associated perturbations
908 result in both upregulation and downregulation of gene modules, consequently affecting a range of
909 cellular processes. This further illuminates the collective behavior of genes within each module,
910 emphasizing either an enhancement or decline of the functional output of co-regulated modules in AD.
911 For instance, in the MTG, the downregulated neuronal modules exclusively comprised downregulated
912 hDEGs and vice versa, implicating these genes in the system-level disruptions of cellular processes,
913 which are essential for normal neuronal functions. This exclusive alignment underscores a strong
914 functional coherence within these modules, suggesting that these hDEGs could be critical regulators in
915 the onset and progression of AD, likely indicating a coordinated modular response to AD. Remarkably,
916 our findings show intriguing patterns of interregional consistency and complexity. Across all brain
917 regions, dysregulated modules exhibited a predominant enrichment for pathways perturbed in a specific
918 direction. Interestingly, while certain DMEs displayed opposing dysregulation patterns relative to their
919 corresponding enriched pathways, others demonstrated concordant dysregulation with enriched
920 processes. Moreover, we observe region-specific counter-directionality of hDEGs in relation to the
921 DMEs in the SFG versus MTG.

922 Our analysis of glial co-expression signatures across the brain regions elucidates the complex and
923 dynamic roles of astrocytes and microglia in AD. We observed that only a single microglial or astrocyte
924 module in each brain region showed significant enrichment for DEGs and reason that these modules
925 represent critical functional drivers of pathway dysregulation. Consistent with this, we observed a
926 significantly reduced number of hDEGs across all glial modules, pointing towards a potentially
927 diminished role of DEGs in orchestrating glial-associated systems-level differences in AD. Contrary to
928 extant narratives that largely assign a neuroinflammatory role to glial cells, our data unveil robust
929 enrichment for AD-related genes involved in a range of biological processes, from synaptic pruning
930 and stress response to glutamate homeostasis and Ca^{2+} signaling. This suggests that alterations in
931 modular gene expression contribute significantly to the pervasive involvement of glial cells in AD.
932 Specifically in microglia, we noted the critical role of modules governing dysregulated immune
933 responses, phagocytic activities, and synaptic function. Such findings underscore the multi-
934 functionality of microglia in AD, highlighting their involvement in preserving neuronal integrity
935 through synaptic maintenance, myelin formation, and other mechanisms. Additionally, our findings
936 reveal the critical role of disease-associated glial states in AD pathology. We observed that hub genes
937 in the AD-enriched glial modules were fundamentally associated with reactive astrocyte and microglia
938 states, indicating that glial cells assume activated states due to the complex systems-level interactions
939 among these genes.

Cross-regional analysis between the MTG, SFG, and ETC, reinforced the theme of overall downregulation of both astrocytic and microglial modules in AD, indicating a prevailing trend of functional repression in these glial cells. These observations collectively strengthen the notion of AD as a systems disease, characterized by tightly linked alterations in gene networks and their associated functional pathways. We also notably identified shared hub genes across these brain regions, with more prominent overlap in neurons. These conserved hubs likely orchestrate directing modular dysregulation and pathway perturbations linked to critical neuronal processes like Ca^{2+} signaling, proteostasis, inflammation, and synaptic function. Though not always differentially expressed themselves, their coordinated behavior within modules may underpin consistent pathway disruptions in AD. Glial cells express more limited overlap, but shared genes govern diverse glial activation-related processes, potentially serving as brain-wide markers for astrocytic or microglial reactivity for disease diagnostics or targeted therapeutic interventions. Nevertheless, experimental validation remains essential to confirm the role of these putative hub genes as conserved, causal drivers of AD pathogenesis. In summary, integrated analyses of cell type-specific co-expression modules across multiple affected brain regions hold significant potential for elucidating key network regulators and pathways that may offer new therapeutic targets for AD.

Conclusions

Our study provides a comprehensive systems-level analysis of the pathway perturbations associated with AD across multiple brain regions and cell types. Leveraging snRNA-seq data, we integrate pathway activity analysis with WGCNA, revealing profound heterogeneity in the dysregulation of biological processes in neurons and glia. Synaptic dysfunction and dysregulated Ca^{2+} signaling emerging as convergent axes of pathogenesis. Surprisingly, we observe limited overlap between DEGs and disrupted gene programs, suggesting DEGs alone do not adequately represent the collective modular alterations driving AD pathology. Indeed, we demonstrate that DEGs have a more pronounced role in driving modular dysregulation in neurons compared to glial cells. We also identified conserved hub genes across modules and brain regions which offers potential brain-wide cell-type-specific therapeutic targets and biomarkers. Overall, these findings underscore the necessity of integrated, systems-oriented models to fully capture the complexity of molecular interactions underlying AD and other polygenic systems neurodegenerative disorders.

973 # List of abbreviations

974 ***AD:*** Alzheimer's Disease

975 ***Aβ:*** Amyloid-beta

976 ***NFTs:*** Neurofibrillary Tangles

977 ***scRNA-seq:*** Single-cell RNA-sequencing

978 ***snRNA-seq:*** Single-nucleus RNA-sequencing

979 ***DEG:*** Differential Gene Expression

980 ***DAM:*** Disease-Associated Microglia

981 ***Ca^{2+}:*** Calcium

982 ***hub-DEGs:*** hub DEGs

983 ***MTG:*** Middle Temporal Gyrus

984 ***SFG:*** Superior Frontal Gyrus

985 ***ETC:*** Entorhinal Cortex

986 ***ADNC:*** AD Neuropathologic Change

987 ***ACT:*** Adult Changes in Thought

988 ***ADRC:*** Alzheimer's Disease Research Center

989 ***NDBB:*** Neurodegenerative Disease Brain Bank

990 ***SEA-AD:*** Seattle Alzheimer's Disease

991 ***GSVA:*** Gene Set Variation Analysis

992 ***WGCNA:*** Weighted Gene Co-expression Analysis

993 ***hdWGCNA:*** High Dimensional Weighted Gene Co-expression Analysis

994 ***ME:*** Module Eigengenes

995 ***DME:*** Differential Module Eigengenes

996 ***VGCC:*** Voltage Gated Calcium Channel

997

Declarations

Data availability

Processed snRNA-seq data and metadata from Leng et al. (20) are available for download at the Synapse portal ((42), under ID syn21788402), under controlled use conditions. Processed data from Gabitto et al. (35) can be freely downloaded without registration from the Seattle Alzheimer's Disease (SEA-AD) Brain Cell portal (45) and a public AWS bucket (43).

Code availability

The codes used for the analyses in this study, along with detailed instructions for reproducing the results presented here will be available on GitHub (https://github.com/TemiLeke/systematic_ad_analysis) upon publication.

Authors' Contributions

All authors read and approved the final manuscript. T.A. and G.U. conceived and presented the idea. T.A. and S.I.I processed the data. T.A. conducted the analysis and wrote the initial draft of the manuscript, with input from S.I.I and G.U. S.I.I. assisted with methodology and analysis. G.U. supervised the study. All authors discussed and interpreted the results.

Competing Interests

The authors declare no competing interests.

Funding

This research was funded by National Institute of Health [R01 AG053988 to GU and Angelo Demuro].

Supplementary Information

Additional File 1

Supplementary Table 1. Sample metadata for all 20 donors, including post-mortem neuropathological assessments, clinical evaluations, and pathological grouping. **Supplementary Tables 2—4.** The table of p-values and log fold changes for all genes included in the differential analysis test across all brain regions (MTG 2; STG 3; ETC 4) and cell types. Supplementary Table 5. Table of pathway renaming conventions. **Supplementary Tables 6—8.** Comprehensive documentation of the pathway analysis results for each brain region (MTG 6; SFG 7; ETC 8) with detailed statistical results (coefficient estimates and p-values) for the prioritized candidate pathways identified across major cell types.

1027 **Supplementary Tables 9—11.** Results from DME analysis for each brain region (MTG 9; SFG 10;
1028 ETC 11) across all cell types. **Supplementary Table 12.** List of overlapping dysregulated pathways
1029 along with corresponding statistics for each cell type. **Supplementary Table 13.** List of hub genes and
1030 hDEGs in each module for all cell types across brain regions. Overlapping hub genes are presented in
1031 **Supplementary Table 14.**

1032

1033 ***Additional File 2***

1034 **Supplementary Fig. 1.** Principal Component Analysis (PCA) of aggregated pseudoreplicates
1035 highlighted with relevant metadata. **Supplementary Fig. 2.** Overlapping dysregulated biological
1036 processes across brain regions. **Supplementary Figs. 3—5.** Soft power thresholds demonstrating a fit
1037 to the scale-free topology model across all cell types in each brain region (MTG 3; SFG 4; ETC 5).
1038 **Supplementary Fig. 6—8.** Dendrograms showing the different co-expression modules resulting from
1039 the network analysis across cell types in each brain region (MTG 6; SFG 7; ETC 8).

1040

1041

1042

1043

1044

1045

1046

1047

1048

1049

1050

1051

1052 # References

1053 1. Ferri CP, Prince M, Brayne C, Brodaty H, Fratiglioni L, Ganguli M, et al. Global
1054 prevalence of dementia: a Delphi consensus study. The Lancet. 2005 Dec
1055 17;366(9503):2112–7.

1056 2. Reitz C, Mayeux R. Alzheimer disease: Epidemiology, diagnostic criteria, risk factors
1057 and biomarkers. Biochemical Pharmacology. 2014 Apr 15;88(4):640–51.

1058 3. Gouras GK, Tampellini D, Takahashi RH, Capetillo-Zarate E. Intraneuronal β-amyloid
1059 accumulation and synapse pathology in Alzheimer's disease. Acta Neuropathol. 2010
1060 May;119(5):523–41.

1061 4. Hyman BT, Van Hoesen GW, Damasio AR, Barnes CL. Alzheimer's Disease: Cell-
1062 Specific Pathology Isolates the Hippocampal Formation. Science. 1984 Sep
1063 14;225(4667):1168–70.

1064 5. Mondragón-Rodríguez S, Basurto-Islas G, Santa-Maria I, Mena R, Binder LI, Avila J, et
1065 al. Cleavage and conformational changes of tau protein follow phosphorylation during
1066 Alzheimer's disease. International Journal of Experimental Pathology. 2008;89(2):81–
1067 90.

1068 6. Vogt LJK, Hyman BT, Van Hoesen GW, Damasio AR. Pathological alterations in the
1069 amygdala in Alzheimer's disease. Neuroscience. 1990 Jan 1;37(2):377–85.

1070 7. Gómez-Isla T, Hollister R, West H, Mui S, Growdon JH, Petersen RC, et al. Neuronal
1071 loss correlates with but exceeds neurofibrillary tangles in Alzheimer's disease. Annals
1072 of Neurology. 1997;41(1):17–24.

1073 8. Mucke L, Selkoe DJ. Neurotoxicity of Amyloid β-Protein: Synaptic and Network
1074 Dysfunction. Cold Spring Harb Perspect Med. 2012 Jul;2(7):a006338.

1075 9. Parodi J, Sepúlveda FJ, Roa J, Opazo C, Inestrosa NC, Aguayo LG. β-Amyloid Causes
1076 Depletion of Synaptic Vesicles Leading to Neurotransmission Failure*. Journal of
1077 Biological Chemistry. 2010 Jan 22;285(4):2506–14.

1078 10. Selkoe DJ. Alzheimer's Disease Is a Synaptic Failure. Science. 2002 Oct
1079 25;298(5594):789–91.

1080 11. Wang M, Li A, Sekiya M, Beckmann ND, Quan X, Schrode N, et al. Molecular
1081 Networks and Key Regulators of the Dysregulated Neuronal System in Alzheimer's
1082 Disease [Internet]. bioRxiv; 2019 [cited 2022 Sep 7]. p. 788323. Available from:
1083 https://www.biorxiv.org/content/10.1101/788323v1

1084 12. Mrdjen D, Fox EJ, Bukhari SA, Montine KS, Bendall SC, Montine TJ. The basis of
1085 cellular and regional vulnerability in Alzheimer's disease. Acta Neuropathol. 2019
1086 Nov;138(5):729–49.

1087 13. Wang X, Michaelis ML, Michaelis EK. Functional Genomics of Brain Aging and
1088 Alzheimer's Disease: Focus on Selective Neuronal Vulnerability. Curr Genomics. 2010
1089 Dec;11(8):618–33.

1090 14. Crist AM, Hinkle KM, Wang X, Moloney CM, Matchett BJ, Labuzan SA, et al.
1091 Transcriptomic analysis to identify genes associated with selective hippocampal
1092 vulnerability in Alzheimer's disease. Nature Communications. 2021;12(1).

1093 15. Roussarie JP, Yao V, Rodriguez-Rodriguez P, Oughtred R, Rust J, Plautz Z, et al.
1094 Selective neuronal vulnerability in Alzheimer's disease: a network-based analysis.
1095 Neuron. 2020 Sep 9;107(5):821-835.e12.

1096 16. Stranahan AM, Mattson MP. Selective vulnerability of neurons in layer II of the
1097 entorhinal cortex during aging and Alzheimer's disease. Neural Plast.
1098 2010;2010:108190.

1099 17. Wang M, Roussos P, McKenzie A, Zhou X, Kajiwara Y, Brennand KJ, et al. Integrative
1100 network analysis of nineteen brain regions identifies molecular signatures and networks
1101 underlying selective regional vulnerability to Alzheimer's disease. Genome Medicine.
1102 2016 Nov 1;8(1):104.

1103 18. Cuevas-Diaz Duran R, González-Orozco JC, Velasco I, Wu JQ. Single-cell and single-
1104 nuclei RNA sequencing as powerful tools to decipher cellular heterogeneity and
1105 dysregulation in neurodegenerative diseases. Frontiers in Cell and Developmental
1106 Biology [Internet]. 2022 [cited 2023 Feb 8];10. Available from:
1107 https://www.frontiersin.org/articles/10.3389/fcell.2022.884748

1108 19. Luquez T, Gaur P, Kosater IM, Lam M, Lee DI, Mares J, et al. Cell type-specific
1109 changes identified by single-cell transcriptomics in Alzheimer's disease. Genome
1110 Medicine. 2022 Nov 30;14(1):136.

1111 20. Leng K, Li E, Eser R, Piergies A, Sit R, Tan M, et al. Molecular characterization of
1112 selectively vulnerable neurons in Alzheimer's disease. Nat Neurosci. 2021
1113 Feb;24(2):276–87.

1114 21. Mathys H, Davila-Velderrain J, Peng Z, Gao F, Mohammadi S, Young JZ, et al. Single-
1115 cell transcriptomic analysis of Alzheimer's disease. Nature. 2019 Jun;570(7761):332–7.

1116 22. Morabito S, Miyoshi E, Michael N, Shahin S, Martini AC, Head E, et al. Single-nucleus
1117 chromatin accessibility and transcriptomic characterization of Alzheimer's disease. Nat
1118 Genet. 2021 Aug;53(8):1143–55.

1119 23. Zhou Y, Song WM, Andhey PS, Swain A, Levy T, Miller KR, et al. Human and mouse
1120 single-nucleus transcriptomics reveal TREM2-dependent and TREM2-independent
1121 cellular responses in Alzheimer's disease. Nat Med. 2020 Jan;26(1):131–42.

1122 24. Grubman A, Chew G, Ouyang JF, Sun G, Choo XY, McLean C, et al. A single-cell atlas
1123 of entorhinal cortex from individuals with Alzheimer's disease reveals cell-type-specific
1124 gene expression regulation. Nat Neurosci. 2019 Dec;22(12):2087–97.

1125 25. Keren-Shaul H, Spinrad A, Weiner A, Matcovitch-Natan O, Dvir-Szternfeld R, Ulland
1126 TK, et al. A Unique Microglia Type Associated with Restricting Development of
1127 Alzheimer's Disease. Cell. 2017 Jun 15;169(7):1276-1290.e17.

26. Habib N, McCabe C, Medina S, Varshavsky M, Kitsberg D, Dvir-Szternfeld R, et al. Disease-associated astrocytes in Alzheimer's disease and aging. Nat Neurosci. 2020 Jun;23(6):701–6.

27. Castrillo JI, Oliver SG. Alzheimer's as a Systems-Level Disease Involving the Interplay of Multiple Cellular Networks. Methods Mol Biol. 2016;1303:3–48.

28. Rayaprolu S, Higginbotham L, Bagchi P, Watson CM, Zhang T, Levey AI, et al. Systems-based proteomics to resolve the biology of Alzheimer's disease beyond amyloid and tau. Neuropsychopharmacol. 2021 Jan;46(1):98–115.

29. Calabrò M, Rinaldi C, Santoro G, Crisafulli C. The biological pathways of Alzheimer disease: a review. AIMS Neurosci. 2020 Dec 16;8(1):86–132.

30. Guo T, Zhang D, Zeng Y, Huang TY, Xu H, Zhao Y. Molecular and cellular mechanisms underlying the pathogenesis of Alzheimer's disease. Molecular Neurodegeneration. 2020 Jul 16;15(1):40.

31. Morabito S, Reese F, Rahimzadeh N, Miyoshi E, Swarup V. hdWGCNA identifies co-expression networks in high-dimensional transcriptomics data. Cell Reports Methods [Internet]. 2023 Jun 12 [cited 2023 Jun 13];0(0). Available from: https://www.cell.com/cell-reports-methods/abstract/S2667-2375(23)00127-3

32. Miyoshi E, Morabito S, Henningfield CM, Rahimzadeh N, Shabestari SK, Das S, et al. Spatial and single-nucleus transcriptomic analysis of genetic and sporadic forms of Alzheimer's Disease [Internet]. bioRxiv; 2023 [cited 2023 Jul 27]. p. 2023.07.24.550282. Available from: https://www.biorxiv.org/content/10.1101/2023.07.24.550282v1

33. Langfelder P, Mischel PS, Horvath S. When Is Hub Gene Selection Better than Standard Meta-Analysis? PLOS ONE. 2013 Apr 17;8(4):e61505.

34. de la Fuente A. From 'differential expression' to 'differential networking' – identification of dysfunctional regulatory networks in diseases. Trends in Genetics. 2010 Jul 1;26(7):326–33.

35. Gabitto MI, Travaglini KJ, Rachleff VM, Kaplan ES, Long B, Ariza J, et al. Integrated multimodal cell atlas of Alzheimer's disease [Internet]. bioRxiv; 2023 [cited 2023 May 9]. p. 2023.05.08.539485. Available from: https://www.biorxiv.org/content/10.1101/2023.05.08.539485v1

36. Hyman BT, Phelps CH, Beach TG, Bigio EH, Cairns NJ, Carrillo MC, et al. National Institute on Aging–Alzheimer's Association guidelines for the neuropathologic assessment of Alzheimer's disease. Alzheimers Dement. 2012 Jan;8(1):1–13.

37. Braak H, Braak E. Development of Alzheimer-related neurofibrillary changes in the neocortex inversely recapitulates cortical myelogenesis. Acta Neuropathol. 1996 Aug;92(2):197–201.

38. Thal DR, Rüb U, Orantes M, Braak H. Phases of Aβ-deposition in the human brain and its relevance for the development of AD. Neurology. 2002 Jun 25;58(12):1791–800.

1167 39. Braak H, Alafuzoff I, Arzberger T, Kretzschmar H, Del Tredici K. Staging of Alzheimer
1168 disease-associated neurofibrillary pathology using paraffin sections and
1169 immunocytochemistry. Acta Neuropathol. 2006 Oct;112(4):389–404.

1170 40. Grinberg LT, Ferretti RE de L, Farfel JM, Leite R, Pasqualucci CA, Rosemberg S, et al.
1171 Brain bank of the Brazilian aging brain study group - a milestone reached and more than
1172 1,600 collected brains. Cell Tissue Bank. 2007;8(2):151–62.

1173 41. Hänzelmann S, Castelo R, Guinney J. GSVA: gene set variation analysis for microarray
1174 and RNA-Seq data. BMC Bioinformatics. 2013 Jan 16;14(1):7.

1175 42. info@sagebase.org SB. Synapse | Sage Bionetworks [Internet]. [cited 2024 Feb 22].
1176 Available from: https://www.synapse.org

1177 43. Seattle Alzheimer's Disease Brain Cell Atlas (SEA-AD) - Registry of Open Data on
1178 AWS [Internet]. [cited 2024 Feb 22]. Available from:
1179 https://registry.opendata.aws/allen-sea-ad-atlas/

1180 44. L. Lun AT, Bach K, Marioni JC. Pooling across cells to normalize single-cell RNA
1181 sequencing data with many zero counts. Genome Biology. 2016 Apr 27;17(1):75.

1182 45. Seattle Alzheimer's Disease Brain Cell Atlas - brain-map.org [Internet]. [cited 2024 Feb
1183 22]. Available from: https://portal.brain-map.org/explore/seattle-alzheimers-
1184 disease/seattle-alzheimers-disease-brain-cell-atlas-download?edit&language=en

1185 46. Squair JW, Gautier M, Kathe C, Anderson MA, James ND, Hutson TH, et al.
1186 Confronting false discoveries in single-cell differential expression. Nat Commun. 2021
1187 Sep 28;12(1):5692.

1188 47. Love MI, Huber W, Anders S. Moderated estimation of fold change and dispersion for
1189 RNA-seq data with DESeq2. Genome Biology. 2014 Dec 5;15(12):550.

1190 48. Xie Z, Bailey A, Kuleshov MV, Clarke DJB, Evangelista JE, Jenkins SL, et al. Gene Set
1191 Knowledge Discovery with Enrichr. Current Protocols. 2021 Mar;1(3):e90.

1192 49. Blanchard JW, Akay LA, Davila-Velderrain J, von Maydell D, Mathys H, Davidson
1193 SM, et al. APOE4 impairs myelination via cholesterol dysregulation in
1194 oligodendrocytes. Nature. 2022 Nov;611(7937):769–79.

1195 50. Subramanian A, Tamayo P, Mootha VK, Mukherjee S, Ebert BL, Gillette MA, et al.
1196 Gene set enrichment analysis: A knowledge-based approach for interpreting genome-
1197 wide expression profiles. Proceedings of the National Academy of Sciences. 2005 Oct
1198 25;102(43):15545–50.

1199 51. Mohammadi S, Davila-Velderrain J, Kellis M. A multiresolution framework to
1200 characterize single-cell state landscapes. Nat Commun. 2020 Oct 26;11(1):5399.

1201 52. Butler A, Hoffman P, Smibert P, Papalexi E, Satija R. Integrating single-cell
1202 transcriptomic data across different conditions, technologies, and species. Nat
1203 Biotechnol. 2018 May;36(5):411–20.

1204 53. Ochoa D, Hercules A, Carmona M, Suveges D, Baker J, Malangone C, et al. The next-
1205 generation Open Targets Platform: reimagined, redesigned, rebuilt. Nucleic Acids
1206 Research. 2023 Jan 6;51(D1):D1353–9.

1207 54. Kanehisa M, Furumichi M, Sato Y, Kawashima M, Ishiguro-Watanabe M. KEGG for
1208 taxonomy-based analysis of pathways and genomes. Nucleic Acids Res. 2023 Jan
1209 6;51(D1):D587–92.

1210 55. Rouillard AD, Gundersen GW, Fernandez NF, Wang Z, Monteiro CD, McDermott MG,
1211 et al. The harmonizome: a collection of processed datasets gathered to serve and mine
1212 knowledge about genes and proteins. Database. 2016 Jan 1;2016:baw100.

1213 56. Law CW, Zeglinski K, Dong X, Alhamdoosh M, Smyth GK, Ritchie ME. A guide to
1214 creating design matrices for gene expression experiments [Internet]. F1000Research;
1215 2020 [cited 2023 Mar 17]. Available from: https://f1000research.com/articles/9-1444

1216 57. Papalexi E, Satija R. Single-cell RNA sequencing to explore immune cell heterogeneity.
1217 Nat Rev Immunol. 2018 Jan;18(1):35–45.

1218 58. Skinnider MA, Squair JW, Foster LJ. Evaluating measures of association for single-cell
1219 transcriptomics. Nat Methods. 2019 May;16(5):381–6.

1220 59. Chen S, Mar JC. Evaluating methods of inferring gene regulatory networks highlights
1221 their lack of performance for single cell gene expression data. BMC Bioinformatics.
1222 2018 Jun 19;19(1):232.

1223 60. van Dam S, Võsa U, van der Graaf A, Franke L, de Magalhães JP. Gene co-expression
1224 analysis for functional classification and gene–disease predictions. Briefings in
1225 Bioinformatics. 2018 Jul 20;19(4):575–92.

1226 61. Langfelder P, Horvath S. WGCNA: an R package for weighted correlation network
1227 analysis. BMC Bioinformatics. 2008 Dec 29;9(1):559.

1228 62. Manczak M, Park BS, Jung Y, Reddy PH. Differential expression of oxidative
1229 phosphorylation genes in patients with Alzheimer's disease: implications for early
1230 mitochondrial dysfunction and oxidative damage. Neuromolecular Med. 2004;5(2):147–
1231 62.

1232 63. Berridge MJ. Calcium hypothesis of Alzheimer's disease. Pflugers Arch. 2010
1233 Feb;459(3):441–9.

1234 64. Liu L, Wu Q, Zhong W, Chen Y, Zhang W, Ren H, et al. Microarray Analysis of
1235 Differential Gene Expression in Alzheimer's Disease Identifies Potential Biomarkers
1236 with Diagnostic Value. Med Sci Monit. 2020 Jan 27;26:e919249-1-e919249-16.

1237 65. Morabito S, Miyoshi E, Michael N, Swarup V. Integrative genomics approach identifies
1238 conserved transcriptomic networks in Alzheimer's disease. Human Molecular Genetics.
1239 2020 Oct 10;29(17):2899–919.

1240 66. Workgroup AACH, Khachaturian ZS. Calcium Hypothesis of Alzheimer's disease and
1241 brain aging: A framework for integrating new evidence into a comprehensive theory of
1242 pathogenesis. Alzheimer's & Dementia. 2017;13(2):178-182.e17.

1243 67. Ceglia I, Reitz C, Gresack J, Ahn JH, Bustos V, Bleck M, et al. APP intracellular
1244 domain/WAVE1 pathway reduces amyloid β production. Nat Med. 2015
1245 Sep;21(9):1054–9.

1246 68. Ochaba J, Monteys AM, O'Rourke JG, Reidling JC, Steffan JS, Davidson BL, et al.
1247 PIAS1 regulates mutant Huntingtin accumulation and Huntington's disease-associated
1248 phenotypes in vivo. Neuron. 2016 May 4;90(3):507–20.

1249 69. He K, Zhang J, Liu J, Cui Y, Liu LG, Ye S, et al. Functional genomics study of protein
1250 inhibitor of activated STAT1 in mouse hippocampal neuronal cells revealed by RNA
1251 sequencing. Aging (Albany NY). 2021 Mar 24;13(6):9011–27.

1252 70. Anderson AG, Rogers BB, Loupe JM, Rodriguez-Nunez I, Roberts SC, White LM, et al.
1253 Single nucleus multiomics identifies ZEB1 and MAFB as candidate regulators of
1254 Alzheimer's disease-specific cis-regulatory elements. Cell Genomics. 2023 Feb
1255 2;100263.

1256 71. Bohush A, Bieganowski P, Filipek A. Hsp90 and Its Co-Chaperones in
1257 Neurodegenerative Diseases. Int J Mol Sci. 2019 Oct 9;20(20):4976.

1258 72. Gonzalez-Rodriguez M, Villar-Conde S, Astillero-Lopez V, Villanueva-Anguita P,
1259 Ubeda-Banon I, Flores-Cuadrado A, et al. Neurodegeneration and Astrogliosis in the
1260 Human CA1 Hippocampal Subfield Are Related to hsp90ab1 and bag3 in Alzheimer's
1261 Disease. Int J Mol Sci. 2021 Dec 23;23(1):165.

1262 73. Labbadia J, Morimoto RI. The biology of proteostasis in aging and disease. Annu Rev
1263 Biochem. 2015;84:435–64.

1264 74. Miron J, Picard C, Labonté A, Auld D, Breitner J, Poirier J, et al. Association of
1265 PPP2R1A with Alzheimer's disease and specific cognitive domains. Neurobiol Aging.
1266 2019 Sep;81:234–43.

1267 75. Del Prete D, Checler F, Chami M. Ryanodine receptors: physiological function and
1268 deregulation in Alzheimer disease. Mol Neurodegener. 2014 Jun 1;9:21.

1269 76. Yao J, Sun B, Institoris A, Zhan X, Guo W, Song Z, et al. Limiting RyR2 Open Time
1270 Prevents Alzheimer's Disease-Related Neuronal Hyperactivity and Memory Loss but
1271 Not β-Amyloid Accumulation. Cell Rep. 2020 Sep 1;32(12):108169.

1272 77. Yao J, Liu Y, Sun B, Zhan X, Estillore JP, Turner RW, et al. Increased RyR2 open
1273 probability induces neuronal hyperactivity and memory loss with or without
1274 Alzheimer's disease-causing gene mutations. Alzheimers Dement. 2022
1275 Nov;18(11):2088–98.

1276 78. Ashraf A, Jeandriens J, Parkes HG, So PW. Iron dyshomeostasis, lipid peroxidation and
1277 perturbed expression of cystine/glutamate antiporter in Alzheimer's disease: Evidence
1278 of ferroptosis. Redox Biol. 2020 May 1;32:101494.

1279 79. Foster EM, Dangla-Valls A, Lovestone S, Ribe EM, Buckley NJ. Clusterin in
1280 Alzheimer's Disease: Mechanisms, Genetics, and Lessons From Other Pathologies.
1281 Frontiers in Neuroscience [Internet]. 2019 [cited 2023 Aug 14];13. Available from:
1282 https://www.frontiersin.org/articles/10.3389/fnins.2019.00164

1283 80. Lazarev VF, Tsolaki M, Mikhaylova ER, Benken KA, Shevtsov MA, Nikotina AD, et
1284 al. Extracellular GAPDH Promotes Alzheimer Disease Progression by Enhancing
1285 Amyloid-β Aggregation and Cytotoxicity. Aging Dis. 2021 Aug 1;12(5):1223–37.

1286 81. Tang L, Wang ZB, Ma LZ, Cao XP, Tan L, Tan MS. Dynamic changes of CSF clusterin
1287 levels across the Alzheimer's disease continuum. BMC Neurol. 2022 Dec 1;22(1):508.

1288 82. Chen T, Gai WP, Abbott CA. Dipeptidyl peptidase 10 (DPP10(789)): a voltage gated
1289 potassium channel associated protein is abnormally expressed in Alzheimer's and other
1290 neurodegenerative diseases. Biomed Res Int. 2014;2014:209398.

1291 83. Malamon JS, Kriete A. Erosion of Gene Co-expression Networks Reveal Deregulation
1292 of Immune System Processes in Late-Onset Alzheimer's Disease. Frontiers in
1293 Neuroscience [Internet]. 2020 [cited 2023 Jul 21];14. Available from:
1294 https://www.frontiersin.org/articles/10.3389/fnins.2020.00228

1295 84. Mitra S, P KB, R SC, Saikumar NV, Philip P, Narayanan M. Alzheimer's disease
1296 rewires gene coexpression networks coupling different brain regions [Internet]. bioRxiv;
1297 2022 [cited 2023 Jul 7]. p. 2022.05.22.492888. Available from:
1298 https://www.biorxiv.org/content/10.1101/2022.05.22.492888v1

1299 85. Xiang J, Wang X, Gao Y, Li T, Cao R, Yan T, et al. Phosphodiesterase 4D Gene
1300 Modifies the Functional Network of Patients With Mild Cognitive Impairment and
1301 Alzheimer's Disease. Front Genet. 2020 Jan 1;11:890.

1302 86. Tibbo AJ, Tejeda GS, Baillie GS. Understanding PDE4's function in Alzheimer's
1303 disease; a target for novel therapeutic approaches. Biochem Soc Trans. 2019 Oct
1304 31;47(5):1557–65.

1305 87. Shi Y, Lv J, Chen L, Luo G, Tao M, Pan J, et al. Phosphodiesterase-4D Knockdown in
1306 the Prefrontal Cortex Alleviates Memory Deficits and Synaptic Failure in Mouse Model
1307 of Alzheimer's Disease. Front Aging Neurosci. 2021 Jan 1;13:722580.

1308 88. Qiang Q, Skudder-Hill L, Toyota T, Wei W, Adachi H. CSF GAP-43 as a biomarker of
1309 synaptic dysfunction is associated with tau pathology in Alzheimer's disease. Sci Rep.
1310 2022 Oct 1;12(1):17392.

1311 89. Sandelius Å, Portelius E, Källén Å, Zetterberg H, Rot U, Olsson B, et al. Elevated CSF
1312 GAP-43 is Alzheimer's disease specific and associated with tau and amyloid pathology.
1313 Alzheimers Dement. 2019 Jan 1;15(1):55–64.

1314 90. Zhu Y, Guo X, Zhu F, Zhang Q, Yang Y, For TADNI. Association of CSF GAP-43 and
1315 *APOE* ε4 with Cognition in Mild Cognitive Impairment and Alzheimer's Disease. Cells.
1316 2022 Dec 1;12(1):13.

1317 91. Fernandez-Enright F, Andrews JL. Lingo-1: a novel target in therapy for Alzheimer's
1318 disease? Neural Regen Res. 2016 Jan;11(1):88–9.

1319 92. Xiang Y, Xin J, Le W, Yang Y. Neurogranin: A Potential Biomarker of Neurological
1320 and Mental Diseases. Frontiers in Aging Neuroscience [Internet]. 2020 [cited 2023 Aug
1321 16];12. Available from: https://www.frontiersin.org/articles/10.3389/fnagi.2020.584743

93. Folts CJ, Giera S, Li T, Piao X. Adhesion G protein-coupled receptors as drug target for neurological diseases. Trends Pharmacol Sci. 2019 Apr;40(4):278–93.

94. Kulczyńska-Przybik A, Dulewicz M, Słowik A, Borawska R, Kułakowska A, Kochanowicz J, et al. The Clinical Significance of Cerebrospinal Fluid Reticulon 4 (RTN4) Levels in the Differential Diagnosis of Neurodegenerative Diseases. J Clin Med. 2021 Nov 13;10(22):5281.

95. Zhang H, Therriault J, Kang MS, Ng KP, Pascoal TA, Rosa-Neto P, et al. Cerebrospinal fluid synaptosomal-associated protein 25 is a key player in synaptic degeneration in mild cognitive impairment and Alzheimer's disease. Alzheimer's Research & Therapy. 2018 Aug 16;10(1):80.

96. Zolochevska O, Bjorklund N, Woltjer R, Wiktorowicz JE, Taglialatela G. Postsynaptic Proteome of Non-Demented Individuals with Alzheimer's Disease Neuropathology. J Alzheimers Dis. 2018 Jan 1;65(2):659–82.

97. Han J, Hyun J, Park J, Jung S, Oh Y, Kim Y, et al. Aberrant role of pyruvate kinase M2 in the regulation of gamma-secretase and memory deficits in Alzheimer's disease. Cell Rep. 2021 Dec 7;37(10):110102.

98. Li Y, Chen Z, Wang Q, Lv X, Cheng Z, Wu Y, et al. Identification of hub proteins in cerebrospinal fluid as potential biomarkers of Alzheimer's disease by integrated bioinformatics. J Neurol. 2023 Mar 1;270(3):1487–500.

99. Traxler L, Herdy JR, Stefanoni D, Eichhorner S, Pelucchi S, Szücs A, et al. Warburg-like metabolic transformation underlies neuronal degeneration in sporadic Alzheimer's disease. Cell Metab. 2022 Sep 1;34(9):1248-1263.e6.

100. Zhou X, Sun L, Bastos de Oliveira F, Qi X, Brown WJ, Smolka MB, et al. Prosaposin facilitates sortilin-independent lysosomal trafficking of progranulin. J Cell Biol. 2015 Sep 1;210(6):991–1002.

101. Mendsaikhan A, Tooyama I, Bellier JP, Serrano GE, Sue LI, Lue LF, et al. Characterization of lysosomal proteins Progranulin and Prosaposin and their interactions in Alzheimer's disease and aged brains: increased levels correlate with neuropathology. Acta Neuropathologica Communications. 2019 Dec 21;7(1):215.

102. Zhang Q, Ma C, Gearing M, Wang PG, Chin LS, Li L. Integrated proteomics and network analysis identifies protein hubs and network alterations in Alzheimer's disease. Acta Neuropathologica Communications. 2018 Mar 1;6(1):19.

103. Anirudhan A, Angulo-Bejarano PI, Paramasivam P, Manokaran K, Kamath SM, Murugesan R, et al. RPL6: A Key Molecule Regulating Zinc- and Magnesium-Bound Metalloproteins of Parkinson's Disease. Front Neurosci. 2021 Mar 11;15:631892.

104. Pollutri D, Penzo M. Ribosomal Protein L10: From Function to Dysfunction. Cells. 2020 Nov 19;9(11):2503.

105. Garcia-Esparcia P, Diaz-Lucena D, Ainciburu M, Torrejón-Escribano B, Carmona M, Llorens F, et al. Glutamate Transporter GLT1 Expression in Alzheimer Disease and Dementia With Lewy Bodies. Front Aging Neurosci. 2018 Jan 1;10:122.

1362 106. Yeung JHY, Palpagama TH, Wood OWG, Turner C, Waldvogel HJ, Faull RLM, et al.
1363 EAAT2 Expression in the Hippocampus, Subiculum, Entorhinal Cortex and Superior
1364 Temporal Gyrus in Alzheimer's Disease. Front Cell Neurosci. 2021 Jan 1;15:702824.

1365 107. Chaudhury AR, Gerecke KM, Wyss JM, Morgan DG, Gordon MN, Carroll SL.
1366 Neuregulin-1 and erbB4 immunoreactivity is associated with neuritic plaques in
1367 Alzheimer disease brain and in a transgenic model of Alzheimer disease. J Neuropathol
1368 Exp Neurol. 2003 Jan 1;62(1):42–54.

1369 108. León A, Aparicio GI, Scorticati C. Neuronal Glycoprotein M6a: An Emerging Molecule
1370 in Chemical Synapse Formation and Dysfunction. Front Synaptic Neurosci. 2021 May
1371 4;13:661681.

1372 109. Liu F, Gong X, Yao X, Cui L, Yin Z, Li C, et al. Variation in the CACNB2 gene is
1373 associated with functional connectivity of the Hippocampus in bipolar disorder. BMC
1374 Psychiatry. 2019 Feb 11;19(1):62.

1375 110. Woo RS, Lee JH, Yu HN, Song DY, Baik TK. Expression of ErbB4 in the apoptotic
1376 neurons of Alzheimer's disease brain. Anat Cell Biol. 2010 Dec 1;43(4):332–9.

1377 111. Woo RS, Lee JH, Yu HN, Song DY, Baik TK. Expression of ErbB4 in the neurons of
1378 Alzheimer's disease brain and APP/PS1 mice, a model of Alzheimer's disease. Anat
1379 Cell Biol. 2011 Jun 1;44(2):116–27.

1380 112. Hüttenrauch M, Ogorek I, Klafki H, Otto M, Stadelmann C, Weggen S, et al.
1381 Glycoprotein NMB: a novel Alzheimer's disease associated marker expressed in a
1382 subset of activated microglia. Acta Neuropathol Commun. 2018 Oct 1;6(1):108.

1383 113. Satoh J ichi, Kino Y, Yanaizu M, Ishida T, Saito Y. Microglia express GPNMB in the
1384 brains of Alzheimer's disease and Nasu-Hakola disease. Intractable Rare Dis Res. 2019
1385 May;8(2):120–8.

1386 114. Smith AM, Davey K, Tsartsalis S, Khozoie C, Fancy N, Tang SS, et al. Diverse human
1387 astrocyte and microglial transcriptional responses to Alzheimer's pathology. Acta
1388 Neuropathol. 2022 Jan 1;143(1):75–91.

1389 115. Zhu Z, Liu Y, Li X, Zhang L, Liu H, Cui Y, et al. GPNMB mitigates Alzheimer's
1390 disease and enhances autophagy via suppressing the mTOR signal. Neurosci Lett. 2022
1391 Jan 1;767:136300.

1392 116. Ando K, Nagaraj S, Küçükali F, de Fisenne MA, Kosa AC, Doeraene E, et al. PICALM
1393 and Alzheimer's Disease: An Update and Perspectives. Cells. 2022 Dec 10;11(24):3994.

1394 117. Xu W, Tan L, Yu JT. The Role of PICALM in Alzheimer's Disease. Mol Neurobiol.
1395 2015 Aug 1;52(1):399–413.

1396 118. Cimino PJ, Sokal I, Leverenz J, Fukui Y, Montine TJ. DOCK2 is a microglial specific
1397 regulator of central nervous system innate immunity found in normal and Alzheimer's
1398 disease brain. Am J Pathol. 2009 Oct;175(4):1622–30.

1399 119. Cimino PJ, Yang Y, Li X, Hemingway JF, Cherne MK, Khademi SB, et al. Ablation of
1400 the Microglial Protein DOCK2 Reduces Amyloid Burden in a Mouse Model of
1401 Alzheimer's Disease. Exp Mol Pathol. 2013 Apr;94(2):366–71.

1402 120. Öhrfelt A, Brinkmalm A, Dumurgier J, Brinkmalm G, Hansson O, Zetterberg H, et al.
1403 The pre-synaptic vesicle protein synaptotagmin is a novel biomarker for Alzheimer's
1404 disease. Alzheimers Res Ther. 2016 Oct 3;8(1):41.

1405 121. Mann CN, Shreedarshanee SD, Kersting CT, Bleem AV, Karch CM, Holtzman DM, et
1406 al. Astrocytic α2-Na+/K+ ATPase inhibition suppresses astrocyte reactivity and reduces
1407 neurodegeneration in a tauopathy mouse model. Sci Transl Med. 2022 Feb
1408 16;14(632):eabm4107.

1409 122. Robinson SR. Neuronal expression of glutamine synthetase in Alzheimer's disease
1410 indicates a profound impairment of metabolic interactions with astrocytes. Neurochem
1411 Int. 2000 Apr 1;36(4–5):471–82.

1412 123. Mendsaikhan A, Tooyama I, Serrano GE, Beach TG, Walker DG. Loss of Lysosomal
1413 Proteins Progranulin and Prosaposin Associated with Increased Neurofibrillary Tangle
1414 Development in Alzheimer Disease. J Neuropathol Exp Neurol. 2021 Aug
1415 10;80(8):741–53.

1416 124. Haydon PG, Carmignoto G. Astrocyte Control of Synaptic Transmission and
1417 Neurovascular Coupling. Physiological Reviews. 2006 Jul;86(3):1009–31.

1418 125. Lian H, Zheng H. Signaling pathways regulating neuron–glia interaction and their
1419 implications in Alzheimer's disease. Journal of Neurochemistry. 2016;136(3):475–91.

1420 126. Stobart J, Anderson C. Multifunctional role of astrocytes as gatekeepers of neuronal
1421 energy supply. Frontiers in Cellular Neuroscience [Internet]. 2013 [cited 2023 Aug
1422 31];7. Available from: https://www.frontiersin.org/articles/10.3389/fncel.2013.00038

1423 127. Iannuzzi F, Sirabella R, Canu N, Maier TJ, Annunziato L, Matrone C. Fyn Tyrosine
1424 Kinase Elicits Amyloid Precursor Protein Tyr682 Phosphorylation in Neurons from
1425 Alzheimer's Disease Patients. Cells. 2020 Jul 1;9(8):E1807.

1426 128. Lau DHW, Hogseth M, Phillips EC, O'Neill MJ, Pooler AM, Noble W, et al. Critical
1427 residues involved in tau binding to fyn: implications for tau phosphorylation in
1428 Alzheimer's disease. Acta Neuropathol Commun. 2016 May 1;4(1):49.

1429 129. Gourmaud S, Paquet C, Dumurgier J, Pace C, Bouras C, Gray F, et al. Increased levels
1430 of cerebrospinal fluid JNK3 associated with amyloid pathology: links to cognitive
1431 decline. J Psychiatry Neurosci. 2015 May;40(3):151–61.

1432 130. Musi CA, Agrò G, Santarella F, Iervasi E, Borsello T. JNK3 as Therapeutic Target and
1433 Biomarker in Neurodegenerative and Neurodevelopmental Brain Diseases. Cells. 2020
1434 Sep 28;9(10):2190.

1435 131. Solas M, Vela S, Smerdou C, Martisova E, Martínez-Valbuena I, Luquin MR, et al. JNK
1436 Activation in Alzheimer's Disease Is Driven by Amyloid β and Is Associated with Tau
1437 Pathology. ACS Chem Neurosci. 2023 Apr 19;14(8):1524–34.

1438 132. De Schepper S, Ge JZ, Crowley G, Ferreira LSS, Garceau D, Toomey CE, et al.
1439 Perivascular cells induce microglial phagocytic states and synaptic engulfment via SPP1
1440 in mouse models of Alzheimer's disease. Nat Neurosci. 2023 Mar;26(3):406–15.

1441 133. Seaman MNJ, Mukadam AS, Breusegem SY. Inhibition of TBC1D5 activates Rab7a
1442 and can enhance the function of the retromer cargo-selective complex. J Cell Sci. 2018
1443 Jun 1;131(12):jcs217398.

1444 134. Barthelson K, Newman M, Lardelli M. Sorting Out the Role of the *Sortilin-Related*
1445 *Receptor 1* in Alzheimer's Disease. J Alzheimers Dis Rep. 2020 May 1;4(1):123–40.

1446 135. Chen SM, Yi YL, Zeng D, Tang YY, Kang X, Zhang P, et al. Hydrogen Sulfide
1447 Attenuates β2-Microglobulin-Induced Cognitive Dysfunction: Involving Recovery of
1448 Hippocampal Autophagic Flux. Front Behav Neurosci. 2019 Jan 1;13:244.

1449 136. Ciarlo E, Massone S, Penna I, Nizzari M, Gigoni A, Dieci G, et al. An intronic ncRNA-
1450 dependent regulation of SORL1 expression affecting Aβ formation is upregulated in
1451 post-mortem Alzheimer's disease brain samples. Dis Model Mech. 2013 Mar
1452 1;6(2):424–33.

1453 137. Gaiser AK, Bauer S, Ruez S, Holzmann K, Fändrich M, Syrovets T, et al. Serum
1454 Amyloid A1 Induces Classically Activated Macrophages: A Role for Enhanced Fibril
1455 Formation. Front Immunol. 2021 Jan 1;12:691155.

1456 138. Hung C, Tuck E, Stubbs V, van der Lee SJ, Aalfs C, van Spaendonk R, et al. SORL1
1457 deficiency in human excitatory neurons causes APP-dependent defects in the
1458 endolysosome-autophagy network. Cell Rep. 2021 Jun 1;35(11):109259.

1459 139. Malik BR, Maddison DC, Smith GA, Peters OM. Autophagic and endo-lysosomal
1460 dysfunction in neurodegenerative disease. Molecular Brain. 2019 Nov 29;12(1):100.

1461 140. Dai DL, Li M, Lee EB. Human Alzheimer's disease reactive astrocytes exhibit a loss of
1462 homeostastic gene expression. Acta Neuropathologica Communications. 2023 Aug
1463 2;11(1):127.

1464 141. Jin J, Liu L, Chen W, Gao Q, Li H, Wang Y, et al. The Implicated Roles of Cell
1465 Adhesion Molecule 1 (CADM1) Gene and Altered Prefrontal Neuronal Activity in
1466 Attention-Deficit/Hyperactivity Disorder: A "Gene–Brain–Behavior Relationship"?
1467 Front Genet. 2019 Sep 26;10:882.

1468 142. Gomez AM, Traunmüller L, Scheiffele P. Neurexins: molecular codes for shaping
1469 neuronal synapses. Nat Rev Neurosci. 2021 Mar;22(3):137–51.

1470 143. Stogsdill JA, Ramirez J, Liu D, Kim YH, Baldwin KT, Enustun E, et al. Astrocytic
1471 neuroligins control astrocyte morphogenesis and synaptogenesis. Nature. 2017 Nov
1472 8;551(7679):192–7.

1473 144. Chung WS, Welsh CA, Barres BA, Stevens B. Do Glia Drive Synaptic and Cognitive
1474 Impairment in Disease? Nat Neurosci. 2015 Nov;18(11):1539–45.

1475 145. Yu Y, Chen R, Mao K, Deng M, Li Z. The Role of Glial Cells in Synaptic Dysfunction:
1476 Insights into Alzheimer's Disease Mechanisms. Aging Dis. 2023 Jul 26;

146. Henstridge CM, Tzioras M, Paolicelli RC. Glial Contribution to Excitatory and Inhibitory Synapse Loss in Neurodegeneration. Frontiers in Cellular Neuroscience [Internet]. 2019 [cited 2023 Sep 4];13. Available from: https://www.frontiersin.org/articles/10.3389/fncel.2019.00063

147. Braak H, Braak E. Neuropathological stageing of Alzheimer-related changes. Acta Neuropathol. 1991 Sep 1;82(4):239–59.

148. Braak H, Braak E. Staging of alzheimer's disease-related neurofibrillary changes. Neurobiology of Aging. 1995 May 1;16(3):271–8.

Supplementary Fig. 1

MTG
Cell Type
Astrocyte
Excitatory
Inhibitory
Microglia
OPC
Oligodendrocyte
Pathology Group
early
late
no
PMI
4.7
5.0
5.03
5.5
6.633333333
7.833333333
10.0
10.2
11.03333333
11.41666667
Age at Death
69
78
81
88
89
90+
PC3
PC2
APOE4 Status
N
Y
Race
asian
white
SFG
Cell Type
Astrocyte
Excitatory
Inhibitory
Microglia
OPC
Oligodendrocyte
Pathology Group
early
late
no
PMI
4.9
6.7
6.9
9.0
12.0
13.0
15.0
30.0
50.0
Age at Death
50
60
71
72
77
82
87
91
PC3
PC2
Braak Stage
0
2
6
ETC
Cell Type
Astrocyte
Excitatory
Inhibitory
Microglia
OPC
Oligodendrocyte
Pathology Group
early
late
no
PMI
4.9
6.7
6.9
9.0
12.0
13.0
15.0
30.0
50.0
Age at Death
50
60
71
72
77
82
87
91
PC3
PC2
Braak Stage
0
2
6

1525

Supplementary Fig. 2

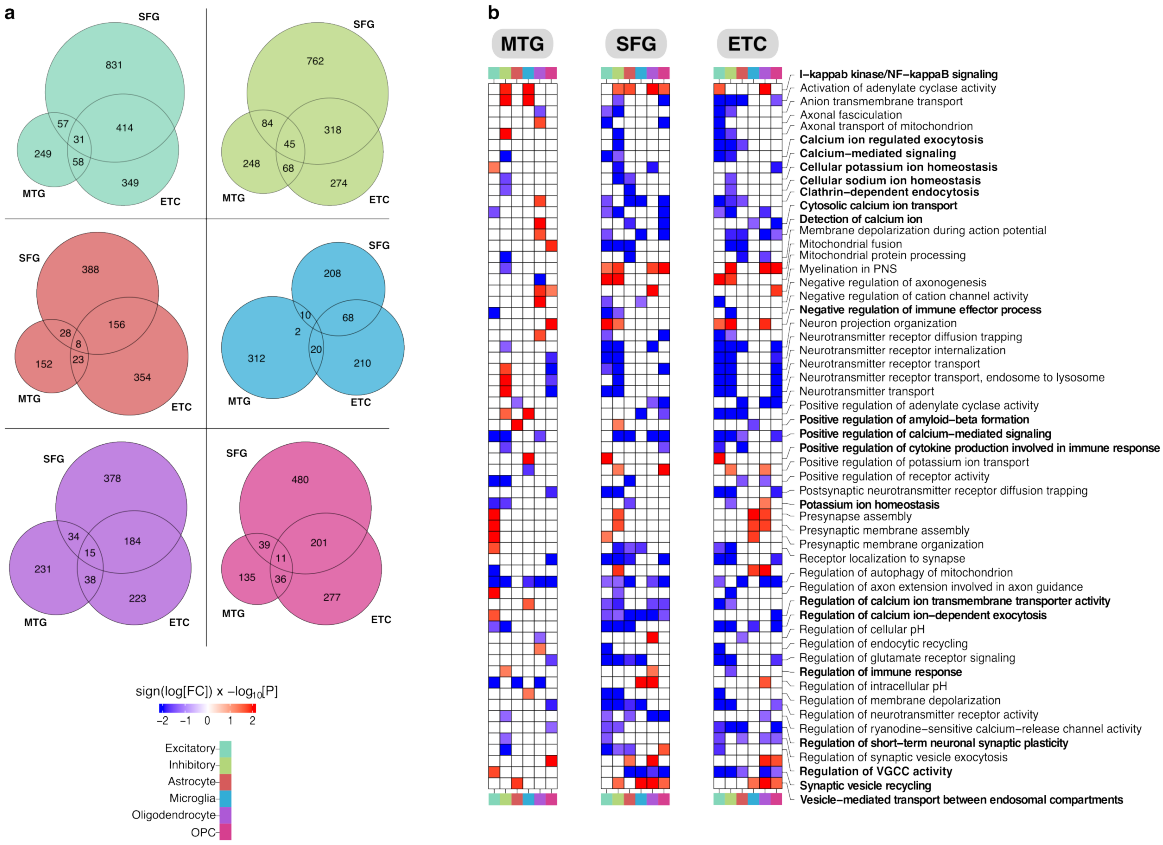

Supplementary Fig. 3

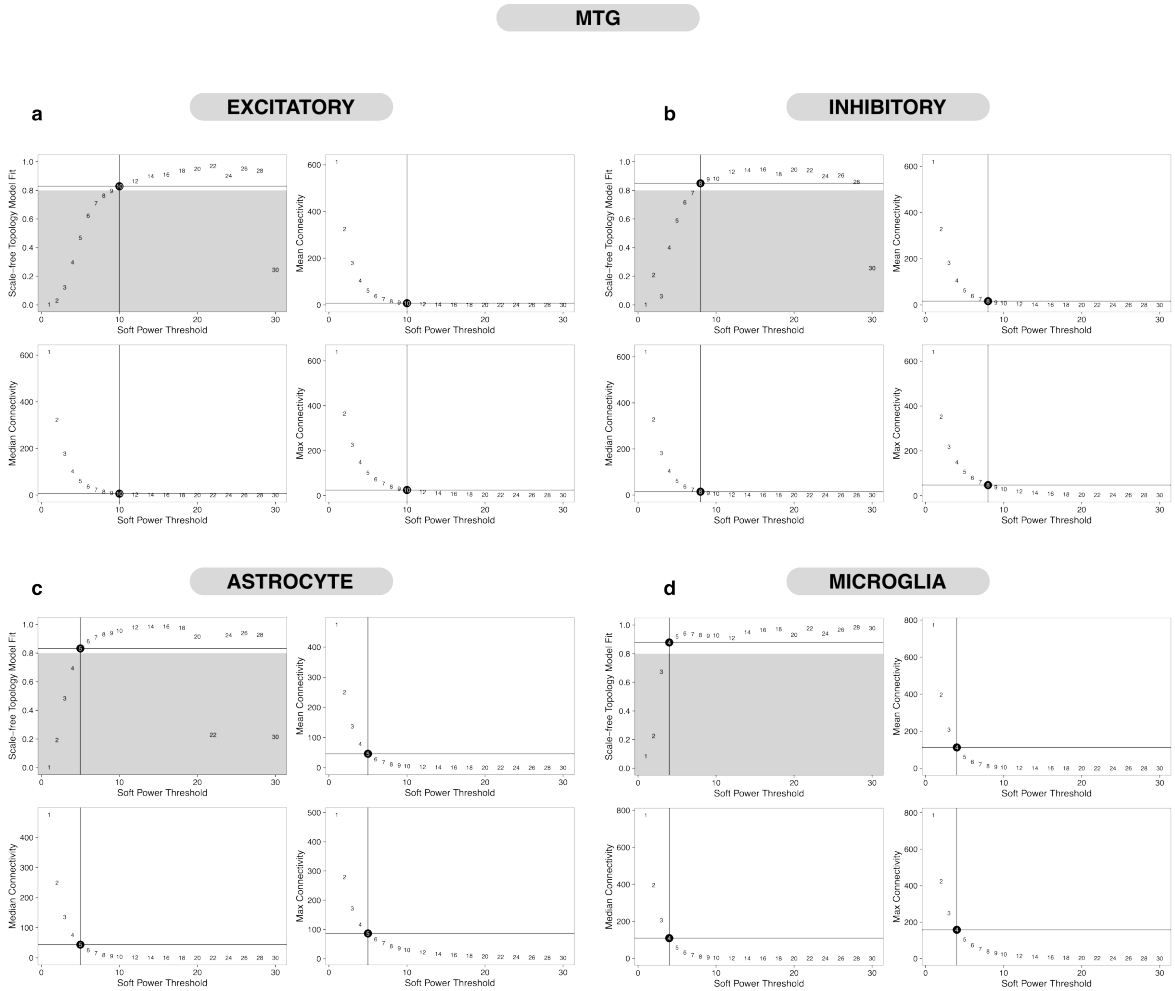

Supplementary Fig. 4

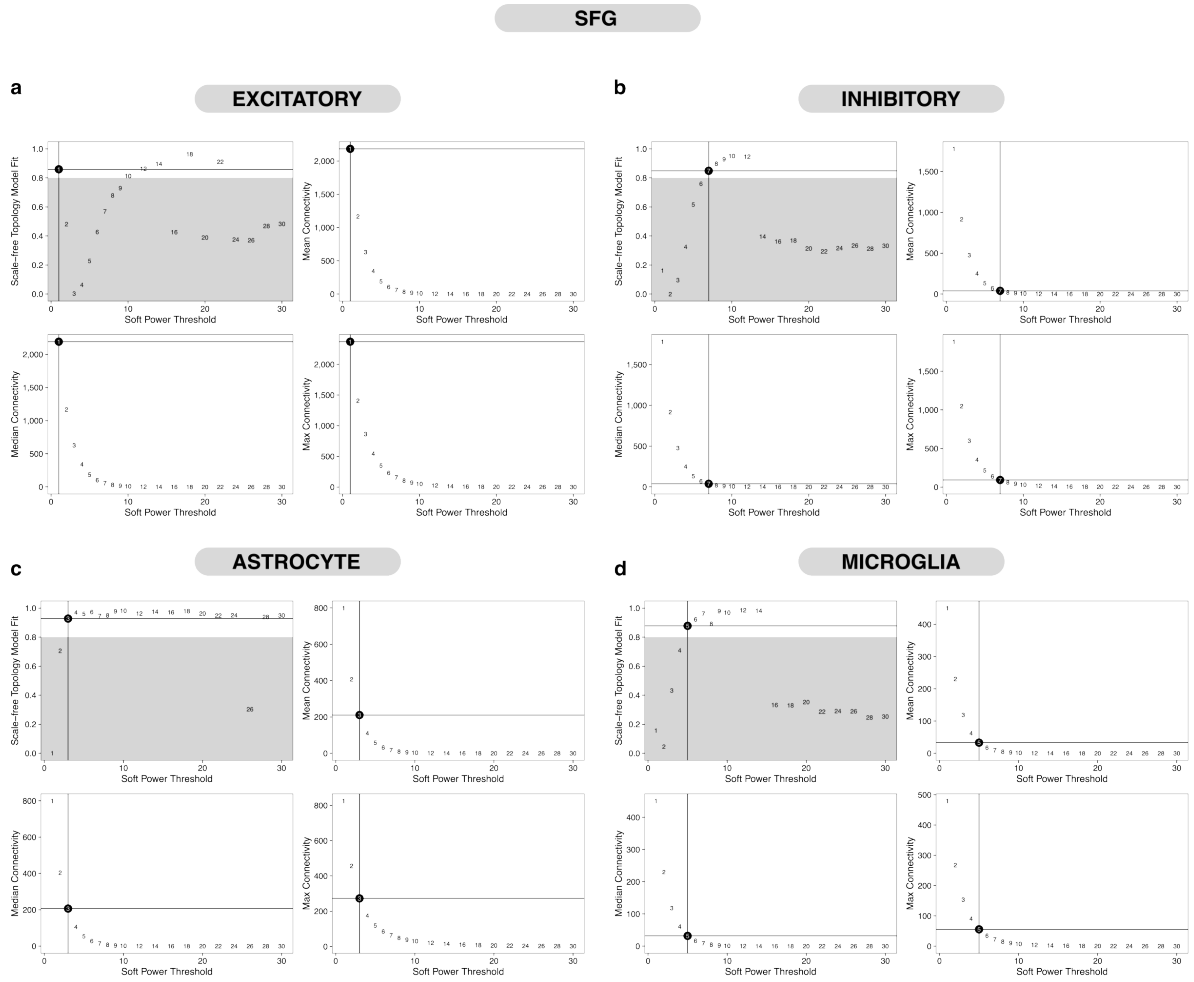

Supplementary Fig. 5

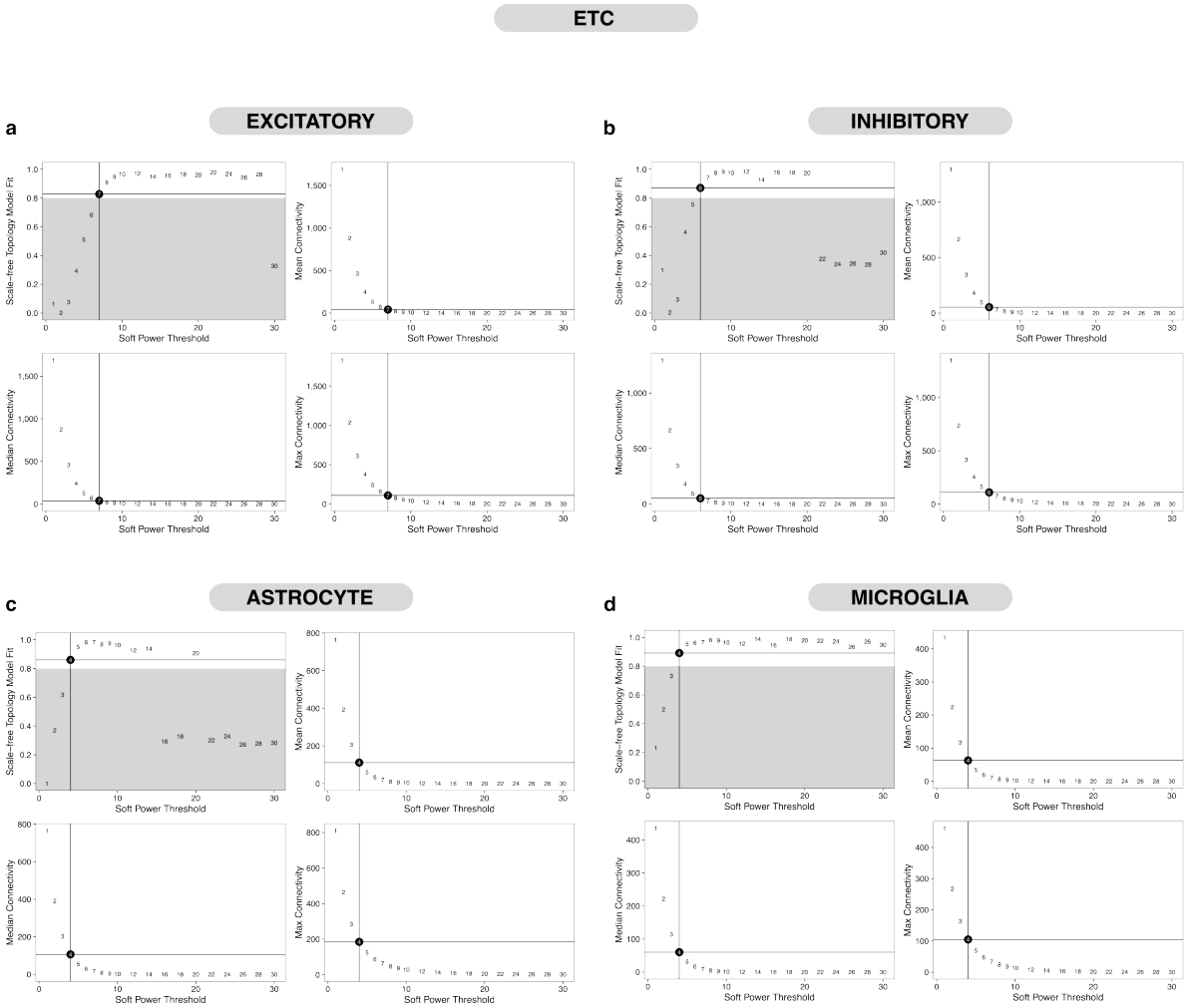

Supplementary Fig. 6

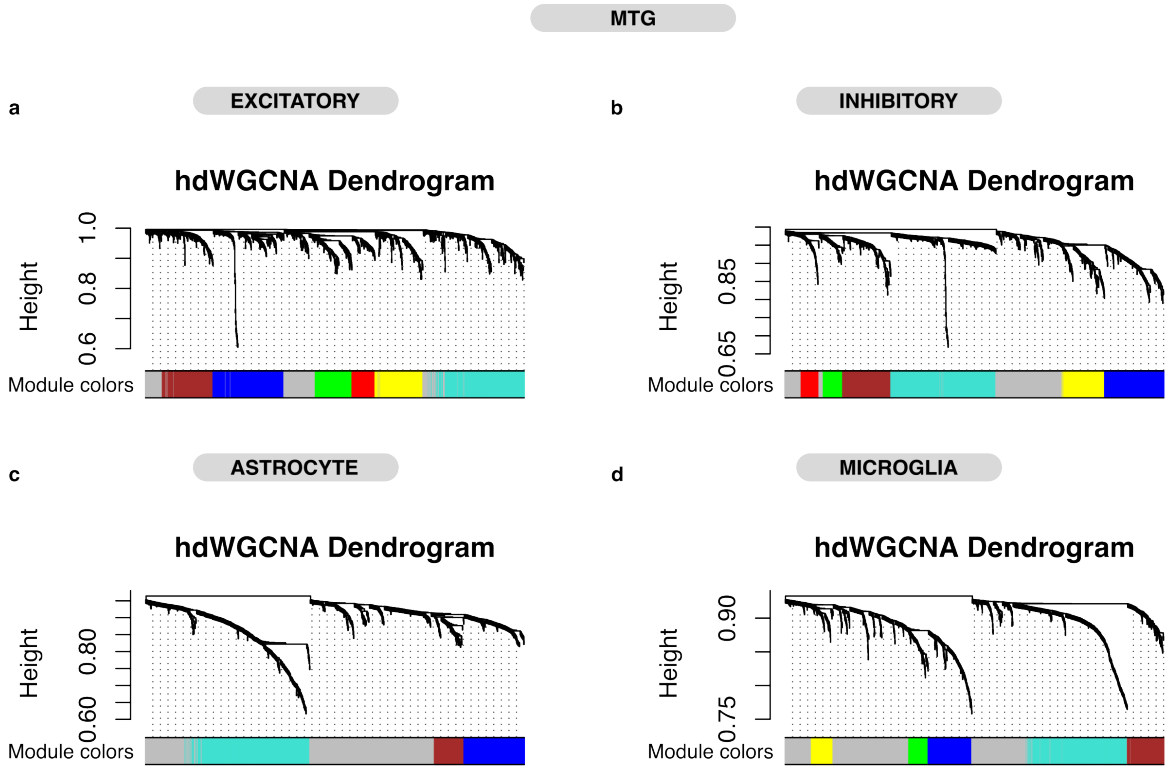

Supplementary Fig. 7

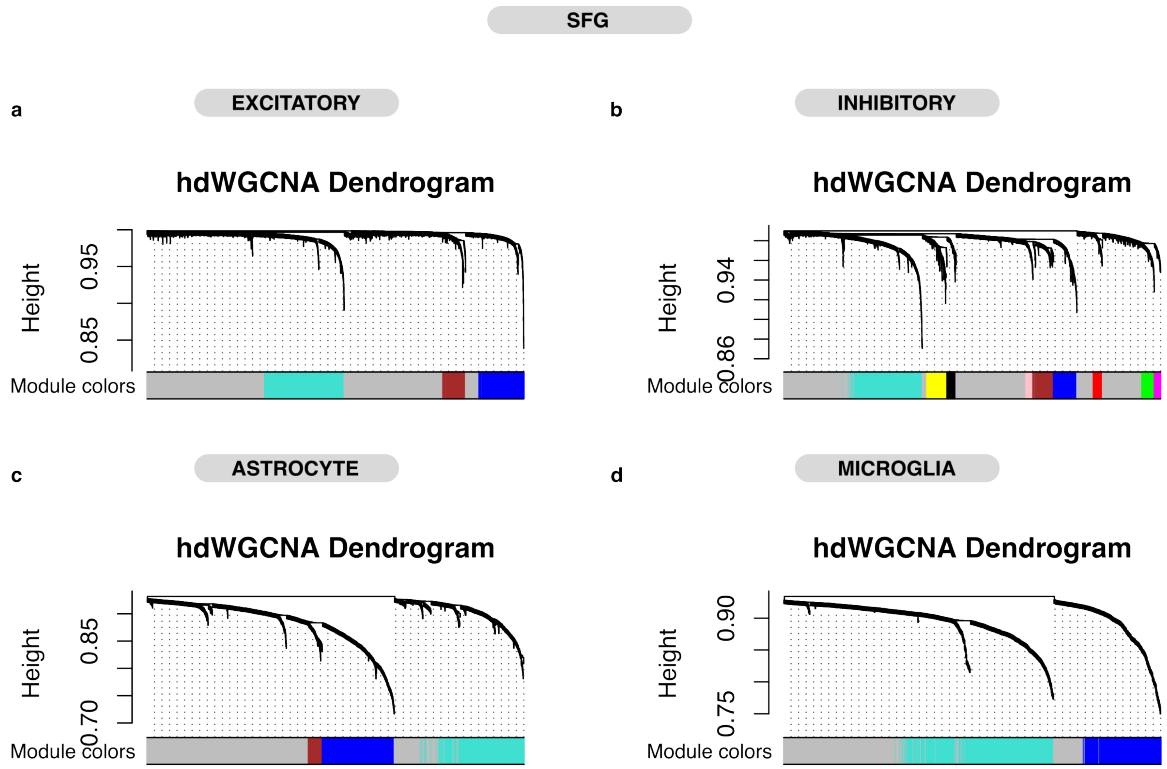
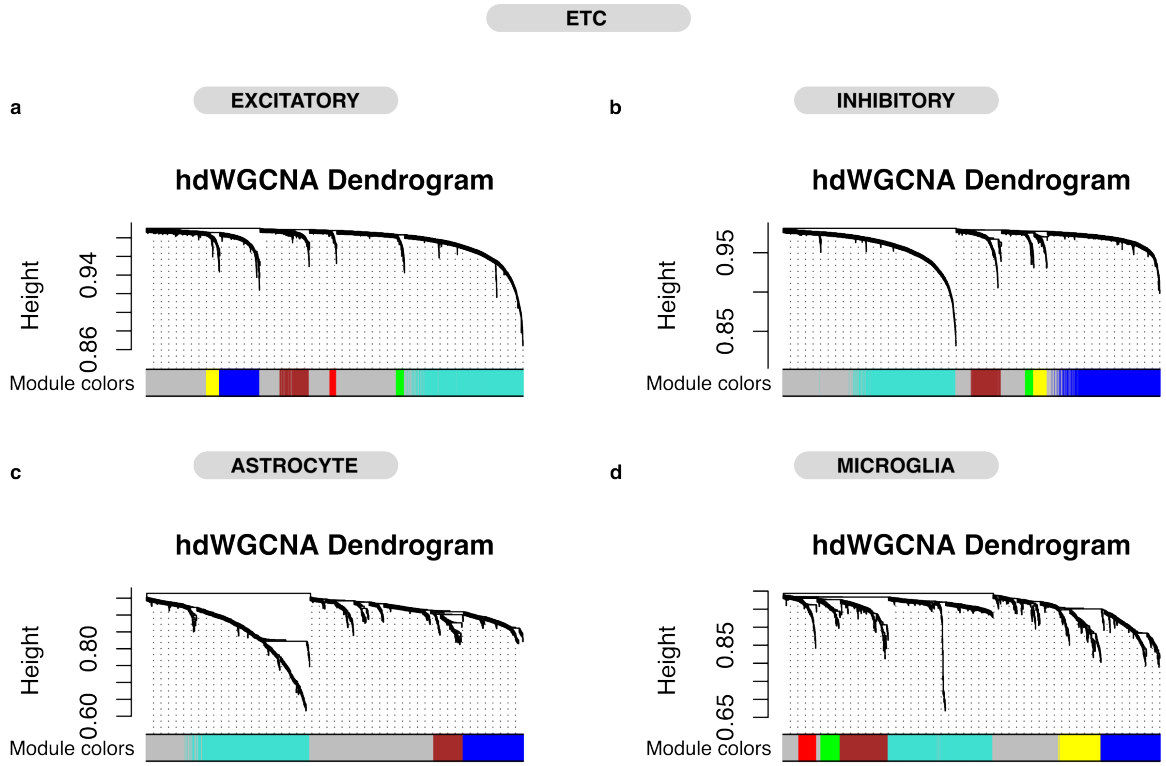
Supplementary Fig. 8